

Thesis

Electron Transport in a Two-Dimensional  
Electron Gas at GaAs/AlGaAs Heterointerface  
under a spatially modulated magnetic field

Mayumi Kato  
Institute for Solid State Physics  
The University of Tokyo

December 1999



# Contents

<b>1</b>	<b>Introduction</b>	<b>5</b>
<b>2</b>	<b>Magneto transport under spatially modulated electric and magnetic fields</b>	<b>9</b>
2.1	Electrostatic potential modulation . . . . .	9
2.2	Magnetic field modulation . . . . .	14
2.3	Coexisting electric and magnetic modulations . . . . .	17
<b>3</b>	<b>The case of out-of-phase electric and magnetic modulations</b>	<b>21</b>
3.1	Introduction . . . . .	21
3.2	Experimental system . . . . .	21
3.3	The control of magnetic field modulation . . . . .	24
3.4	The control of electric field modulation . . . . .	28
	References . . . . .	31
<b>4</b>	<b>Electron-electron umklapp process in 2DEG under a spatially alternating magnetic field</b>	<b>33</b>
4.1	Introduction . . . . .	33
4.2	Theory -Temperature dependence of electron lifetime- . . . . .	34
4.3	The observation of $T^2$ -dependence of resistivity . . . . .	36
4.4	The electron density dependence of e-e scattering . . . . .	41
4.5	Electron temperature dependence of electron-electron scattering	45
4.6	Transverse resistance in oblique lateral superlattice . . . . .	47
	References . . . . .	53
<b>5</b>	<b>Conclusion</b>	<b>55</b>



# Chapter 1

## Introduction

Recent progress in epitaxial growth and micro-fabrication techniques has enabled us to design novel artificial stages for the study of basic electronic processes in condensed matters. Two-dimensional electron gas (2DEG) at the GaAs/AlGaAs hetero-interface offers a particularly well-defined stage for transport studies. The reason lies in the following features of the GaAs/AlGaAs 2DEG system.

1. The system is as close as one could hope, to the free electron picture.

As far as low energy phenomena are concerned, the energy band of the system is isotropic in  $\mathbf{k}$ -space and takes the form of  $\epsilon(\mathbf{k}) = \frac{\hbar^2 k^2}{2m^*}$ ,  $m^* = 0.067m_0$  being the effective mass for the GaAs conduction band. In state of the art samples, the mean free path of electrons exceeds  $10^{-4}\text{m}$  at low temperature. The achievement of high electron mobility owes much to the development of the molecular beam epitaxy (MBE) growth and the modulation doping technique.

2. The electron density can be tuned within a single sample.

The electron density is typically  $n_e \sim 10^{15} - 10^{16}\text{m}^{-2}$ , the Fermi wave length is  $k_F \sim 10^8\text{m}^{-1}$  and the Fermi velocity is  $v_F \sim 10^5\text{m/s}$ . We can control the electron density of a sample by applying a gate bias or by illuminating with an LED (persistent photo conductivity).

3. A tailored potential can be applied to the 2DEG by microfabrication.

We can fabricate a microstructure on the surface of the GaAs/AlGaAs structure and create an artificial potential profile for the 2DEG. The idea of an artificial potential modulation dates back almost a few decades. The work was motivated by the notion that the artificial potential should induce a spectrum of minibands and minigaps, which depends on the potential amplitude

and profile.

The influence of a magnetic field on transport has been intensively studied by many groups in order to reveal complex structures of the spectrum. One of the remarkable phenomena using an artificial potential is a magnetoresistance oscillation due to the commensurability between the cyclotron radius and the potential periodicity. The one observed using a one-dimensional electrostatic potential modulation is called "Weiss oscillation" [1–3]. Weiss *et al.*[1] used an ingenious technique to impose a one-dimensional weak periodic potential modulation on a 2DEG and showed the formation of minibands by the magnetotransport experiment.

Experimentally the substitution magnetic field modulation for potential one could be achieved [10–12]. The advantage of using magnetic modulation is that it allows us to change the modulation amplitude without affecting the density of 2DEG. This is a crucial point in addressing the issue of the electron-electron scattering.

Electron-electron interaction is one of the most essential processes in condensed matter physics. Although there has been much progress in the understanding of the issue in so-called strongly correlated electron systems such as heavy fermion metals, transition metal oxides and organic conductors, a truly quantitative comparison between theory and experiment seems difficult at the moment, because a full treatment of the relevant electron-electron process requires detailed knowledge of the complex band structure of real materials and the Umklapp matrix element. It is desirable, thus, to find a simplest possible experimental system that exhibits the phenomenon at issue.

The system under a magnetic modulation can be the ideal test ground for quantitative study of electron-electron interaction. Therefore we focus upon the transport in 2DEG under a spatially modulated magnetic field in this work. We restrict ourselves to the case of regular periodic structure in one direction, *i.e.* one-dimensional modulation.

The organization of this thesis is as follows. In the next chapter, we describe Weiss oscillation and demonstrate the way how the electrostatic and magnetic modulations can be controlled. In Chapter 3, we show the system which is used in the work described in the subsequent chapters. In Chapter 4 which is main part of this thesis, we address ourselves to the effect of electron-electron scattering in the system. We show that the present system

is well suited to quantitative evaluation of the electron-electron scattering process in the 2DEG. Chapter 5 gives the summary and concluding remarks.



# Chapter 2

## Magneto transport under spatially modulated electric and magnetic fields

### 2.1 Electrostatic potential modulation

One of the phenomena observed in a two-dimensional electron gas (2DEG) under a spatially modulated electro-static and/or magnetic field is a magnetoresistance oscillation due to the commensurability between the cyclotron radius and the potential periodicity. The one observed using a one-dimensional electro-static potential modulation is called "Weiss oscillation" [1–3]. The electrostatic potential modulation is obtained by applying bias voltage to the periodic metallic gate as shown in Fig. 2.1. The effect manifests itself as oscillation of  $\rho_{xx}(B)$ , which is periodic in  $1/B$ . Here,  $x$  is the direction of the potential modulation. Figure 2.2 shows the magnetoresistance oscillations ( $B \leq 0.4\text{T}$ ) [2]. The minima of  $\rho_{xx}(B)$  occur at

$$\frac{2R_c}{a} = n + \varphi, \quad n = 1, 2, 3, \dots \quad (2.1)$$

---

The content of this chapter was reported in M. Kato, A. Endo and Y. Iye: J. Soc. Jpn. **66** 3178 (1997); M. Kato, A. Endo, S. Katsumoto and Y. Iye: PHYSICA B **249-251** 753 (1998); M. Kato, A. Endo, S. Katsumoto and Y. Iye: Solid State Electronics **42**, No.7-8 1121 (1998)

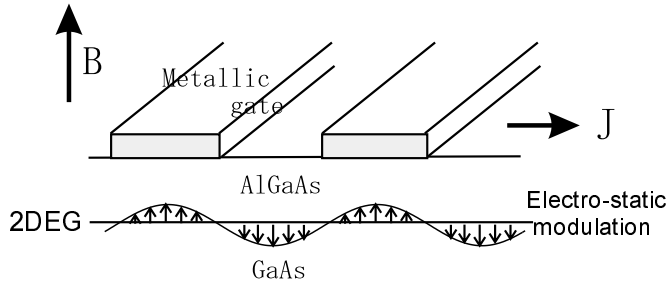


**Figure 2.1:** Schematic drawing of 2DEG with a periodic metallic gate. Electrostatic modulation is created by applying a bias voltage to the gate .

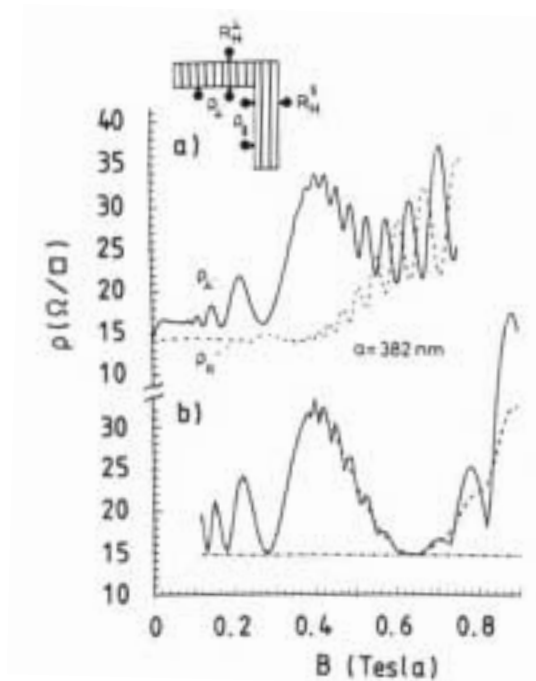


**Figure 2.2:** Magnetoresistance for current perpendicular ( $\rho_{\perp}$ , solid line) and parallel ( $\rho_{\parallel}$ , dash-dotted line) as indicated in the inset, for a sample with  $n_e = 3.16 \times 10^{15} \text{ m}^{-2}$ ,  $\mu = 130 \text{ m}^2/\text{Vs}$ , and  $a = 382 \text{ nm}$  (a) measured temperature  $T = 2.2 \text{ K}$ , (b) calculated for  $T = 2.2 \text{ K}$  and  $4.2 \text{ K}$  ( $\rho_{\perp}$ , dashed line);  $\rho_{\parallel}$  shows no temperature dependence, using  $V_0 = 0.3 \text{ meV}$  [2].

Here,  $a$  is the modulation period,  $R_c \equiv \hbar k_F / eB = \sqrt{2\pi n_e \ell^2}$  is the cyclotron radius of an electron at the Fermi surface,  $k_F = \sqrt{2\pi n_e}$  is the Fermi wave number,  $n_e$  is the electron density, and  $\ell \equiv \sqrt{\hbar / eB}$  is the magnetic length. The *phase term*,  $\varphi$  is equal to  $-1/4$  for the case of electrostatic potential modulation.

The occurrence of minima in  $\rho_{xx}$  is interpreted in the following way. We consider a 2DEG, in the  $x, y$ -plane, subjected to a magnetic field  $\mathbf{B}$  along the  $z$  direction, and an one-dimensional weak periodic potential  $U(x)$  along the  $x$  direction. The one-electron Hamiltonian is

$$H = \frac{1}{2m^*} (\mathbf{P} + e\mathbf{A})^2 + U(x) \quad (2.2)$$

where  $\mathbf{P}$  is the momentum operator,  $m^*$  is the effective mass and  $\mathbf{A}$  is chosen in the Landau gauge  $\mathbf{A} = (0, Bx, 0)$ . In the absence of the modulation, i.e., for  $U(x) = 0$ , the normalized eigen functions of eq. (2.2) are given by  $\phi_n(x + x_0) \exp(iyk_y) / \sqrt{L_y}$ , where  $\phi_n(x)$  is the harmonic-oscillator wave function for the Landau level index  $n$  centered at  $x_0 = \ell^2 k_y$  and  $L_y$  is the length of the 2DEG in the  $y$  direction. The corresponding eigenvalue is  $E_n = (n + 1/2)\hbar\omega_c$ , which is degenerate with respect to the wave vector  $k_y$  ( $\omega_c = eB/m^*$  is the cyclotron frequency).

The modulation potential is approximated by the first Fourier component of the periodic potential, i.e.,  $U(x) = V_0 \cos 2\pi x/a$ , which is expected to be a good approximation for the one induced by the metallic gate on the sample surface. In this case, the exact eigenstates of eq. (2.2) are difficult to obtain in a closed analytical form. The amplitude of the potential modulation  $V_0$  estimated in the reported experiments is so small that we can evaluate the correction to the energy levels by first-order perturbation theory using the unperturbed wave functions given above. We obtain

$$E_{n,k_y} = \left(n + \frac{1}{2}\right) \hbar\omega_c + V_0 e^{-u/2} L_n(u) \cos Kx_0 \quad (2.3)$$

where  $K = 2\pi/a$ ,  $u = K^2 \ell^2 / 2$  and  $L_n(u)$  is the Laguerre polynomial of  $n$ -th order, which oscillates as a function of its index  $n$ . The calculated energy bands  $E_{n,k_y}$  is plotted in Fig. 2.3. The potential  $U(x)$  lifts the degeneracy of the Landau levels, and yields eigenstates  $|x_0, n\rangle$  which carry current in the  $y$  direction,

$$\langle x_0, n | v_y | x_0, n \rangle = \frac{1}{\hbar} \frac{\partial E_{n,k_y}}{\partial k_y}, \quad (2.4)$$

whereas  $\langle x_0, n | v_x | x_0, n \rangle = 0$ . This is the origin of the anisotropic transport coefficients observed in Fig. 2.2.

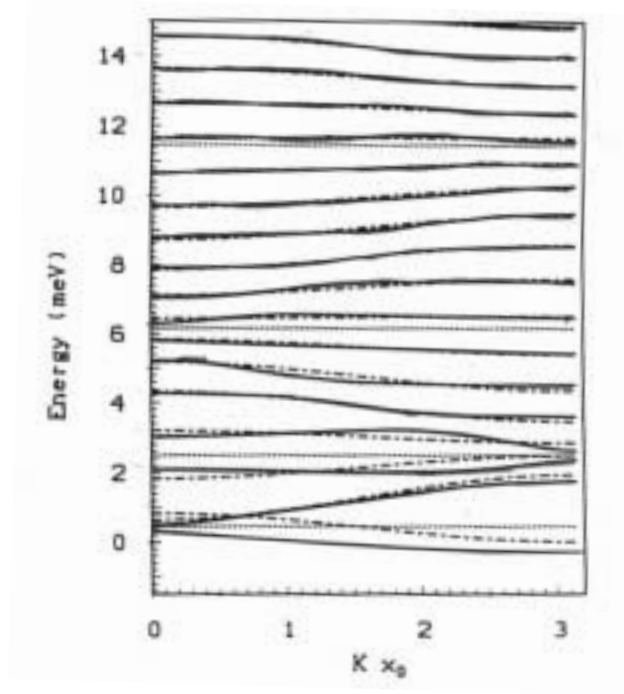


**Figure 2.3:** Calculated energy bands  $E_{n,k_y}$  for  $B=0.5\text{T}$ ,  $V_0=1.5\text{meV}$ ,  $a=100\text{nm}$ , and material parameters of GaAs: solid lines, numerical diagonalization; thick dotted lines, first order approximation; thin dotted lines, energies of zero bandwidth [2].

The instant position of a cyclotron orbiting electron can be written as  $(x(t), y(t)) = (x_0 + R_c \cos \omega_c t, y_0 + R_c \sin \omega_c t)$ . The time average of  $E_{n,k_y}$  is obtained by integrating eq.(2.3) along the cyclotron orbit,

$$\begin{aligned} E_{N_F, k_y} &= \left(N_F + \frac{1}{2}\right) \hbar \omega_c + \frac{1}{2\pi} \int_0^{2\pi} V_0 \cos(K(x_0 + R_c \cos \omega_c t)) d(\omega_c t) \\ &= \left(N_F + \frac{1}{2}\right) \hbar \omega_c + V_0 J_0(K R_c) \cos K x_0, \end{aligned} \quad (2.5)$$

where  $N_F$  is Landau index at the Fermi level and  $J_0(x)$  is the Bessel function of zero-th order. The flat band condition of eq.(2.5),  $J_0(K R_c) = 0$ , is

$$\frac{2R_c}{a} \sim n - \frac{1}{4} \quad n = 1, 2, 3... \quad (2.6)$$

This leads to quenching of drift motion, *i.e.*  $v_x = v_y = 0$ , therefore, the suppression of  $\sigma_{yy}$  causes the minima of  $\rho_{xx}$ .

In another point of view[4], the periodic potential makes spatially modulated electric field  $E_x(x) = \frac{1}{e} \frac{dU(x)}{dx} = \frac{KV_0}{e} \sin Kx$ . An electron acquires local drift velocity  $\mathbf{v}^{drift} = (\mathbf{E} \times \mathbf{B})/B^2 = (0, \frac{KV_0}{eB} \sin Kx)$  as illustrated in Fig. 2.4. Its time average is

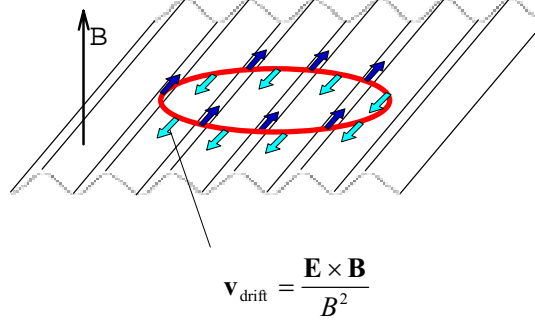


**Figure 2.4:** Potential grating with a cyclotron orbit superimposed. An electron has local drift velocity  $\mathbf{v}^{drift} = (\mathbf{E} \times \mathbf{B})/B^2$

$$\langle v_y^{drift} \rangle = \frac{KV_0}{eB} J_0(KR_c) \sin Kx_0. \quad (2.7)$$

The condition  $\langle v_y^{drift} \rangle = 0$  is again given by eq.(2.6). In this case, the conductivity  $\sigma_{yy}$  becomes zero and leads to the minima of resistivity  $\rho_{xx}$  ( $\rho_{xx} \propto \sigma_{yy}/\sigma_{xy}^2$ ). The magnetoresistance oscillation is explained as a geometrical resonance between the cyclotron motion and potential period.

Next we show expressions for the conductivity of this system[5]. In the absence of the modulation we have electron group velocity  $v_x = v_y = 0$ . Since the presence of the modulation lifts the  $k_y$  degeneracy, we find

$$v_y = \frac{1}{\hbar} \frac{\partial E_{n,k_y}}{\partial k_y} = -\frac{2V_0}{\hbar K} u e^{-u/2} L_n(u) \sin Kx_0 \quad (2.8)$$

while  $v_x = 0$ . The fact that  $v_y$  is no longer zero gives the contribution  $\sigma_{\mu\nu}$  to the conductivity. It takes the form

$$\sigma_{\mu\nu}(\omega) = \frac{2e^2\hbar}{iL_xL_y} \sum_{\alpha\alpha'} \frac{f(E_\alpha) - f(E_{\alpha'})}{(E_\alpha - E_{\alpha'})(E_\alpha - E_{\alpha'} + \hbar\omega + i0^+)} \times \langle \alpha | v_\mu | \alpha' \rangle \langle \alpha' | v_\nu | \alpha \rangle \quad (2.9)$$

which is given by the well-known Kubo-Greenwood formula. By using simple damping approximation  $\omega \rightarrow i/\tau$ , we find

$$\sigma_{yy} = \frac{2e^2\hbar}{iL_xL_y} \frac{\tau}{i\hbar} \sum_{n,x_0} \frac{df(E)}{dE} \Big|_{E=E_n(x_0)} |\langle x_0, n | v_y | x_0, n \rangle|^2$$

$$= 2 \frac{e^2}{\hbar} \frac{2\pi^2}{\hbar} \frac{\ell^2}{a^2} \tau V_0^2 e^{-u} \times \sum_{n=0}^{\infty} [L_n(u)]^2 \left[ -\frac{\partial f(E)}{\partial E} \right]_{E=E_n}. \quad (2.10)$$

The asymptotic expression for  $\sigma_{yy}$  is

$$\frac{\sigma_{yy}}{\sigma_0} = \frac{V_0}{E_F} \frac{V_0}{\hbar\omega_c} \frac{2}{ak_F} \left[ F - 2e^{-\pi/\omega_c\tau_f} A(T/T_c) \cos\left(\frac{2\pi E_F}{\hbar\omega_c}\right) \cos^2\left(\frac{2\pi R_c}{a} - \frac{\pi}{4}\right) \right] \quad (2.11)$$

where  $\tau_f$  the quantum life time,  $\sigma_0 = n_e e^2 \tau / m^*$  the conductivity at zero magnetic field,

$$\begin{aligned} F &= \frac{1}{2} [1 - A(T/T_a)] + A(T/T_a) \cos^2\left(\frac{2\pi R_c}{a} - \frac{\pi}{4}\right), \\ A(x) &= \frac{x}{\sinh x}, \\ k_B T_a &= \frac{\hbar\omega_c}{4\pi^2} ak_F, \\ k_B T_c &= \frac{\hbar\omega_c}{2\pi^2}, \\ \text{and } \frac{\rho_{xx}}{\rho_0} &= [1 + (\omega_c\tau)^2] \frac{\sigma_{yy}}{\sigma_0}. \end{aligned}$$

The second term in eq. (2.11) gives the additional contribution to Shubnikov-de Haas (SdH) oscillations. The first term  $F$  corresponds to the Weiss oscillation. The minima of the term  $F$  occurs when  $\cos^2\left(\frac{2\pi R_c}{a} - \frac{\pi}{4}\right) = 0$ , which leads to eq. (2.6).

The amplitude of the SdH oscillation is determined by the characteristic temperature  $T_c$  while that of the Weiss oscillation is governed by  $T_a$ . Since  $T_a$  is much higher than  $T_c$  for typical experimental conditions, the Weiss oscillation is more robust against temperature than the SdH oscillations.

## 2.2 Magnetic field modulation

Following discovery of the Weiss oscillation effect due to the electrostatic potential modulation, a magnetic field analog of the effect was pursued [6–9]. Theories predict a similar magnetoresistance oscillation except that the *phase term* in eq.(2.1) becomes  $\varphi = +1/4$ . Magnetic Weiss oscillation was observed experimentally [10–12]. In those experiments, a spatially varying magnetic field was produced by placing a suitably micro-patterned ferromagnet or superconductor on the surface of the 2DEG specimen. P. D. Ye *et. al.* [11] used ferromagnetic dysprosium metal gates, while S. Izawa *et. al.* [10] at

our group used nickel to modulate the magnetic field. H. A. Carmona *et. al.* [12] followed a different path and used superconducting stripes.

We consider a 2DEG subjected to the magnetic field  $\mathbf{B}=(B+B_0 \cos Kx)\hat{\mathbf{z}}$ . The corresponding vector potential  $\mathbf{A}$  in the Landau gauge is  $\mathbf{A}=[0, Bx + (B_0/K) \sin Kx, 0]$ . The one-electron Hamiltonian is

$$H = \frac{1}{2m^*} [p_x^2 + (p_y + eBx)^2] + (\omega_0/K)(p_y + eBx) \sin Kx + (m^* \omega_0^2/4K^2)(1 - \cos 2Kx). \quad (2.12)$$

where  $\omega_0 = eB_0/m^*$ ,  $\omega_c = eB/m^*$ . We consider the case where the modulation amplitude is much smaller than the uniform magnetic field ( $B_0 \ll B$ ). By using a first-order perturbation theory, we obtain

$$\begin{aligned} E_{n,k_y} &= \left(n + \frac{1}{2}\right) \hbar\omega_c + \hbar\omega_0 G_n(u) \cos Kx_0 \\ &\quad + (m^* \omega_0^2/4K^2)[1 - e^{-2u} L_n(4u) \cos 2Kx_0] \\ G_n(u) &= e^{-u/2}[L_n(u)/2 + L_{n-1}^1(u)]. \end{aligned} \quad (2.13)$$

Here,  $u = K^2 \ell^2/2$ ,  $L_n(u)$  is the n-th order Laguerre polynomial. We find

$$v_y = \frac{1}{\hbar} \frac{\partial E_{n,k_y}}{\partial k_y} = -\frac{2\omega_0}{K} u G_n(u) \sin Kx_0 \quad (2.14)$$

while  $v_x = 0$ .

The same procedure as that used to obtain eq. (2.11) gives

$$\frac{\sigma_{yy}}{\sigma_0} = \frac{ak_F \hbar\omega_0}{2\pi^2 \hbar\omega_c E_F} \left[ G - 2e^{-\pi/\omega_c \tau_f} A(T/T_c) \cos\left(\frac{2\pi E_F}{\hbar\omega_c}\right) \sin^2\left(\frac{2\pi R_c}{a} - \frac{\pi}{4}\right) \right] \quad (2.15)$$

where

$$G = \frac{1}{2}[1 - A(T/T_a)] + A(T/T_a) \sin^2\left(\frac{2\pi R_c}{a} - \frac{\pi}{4}\right).$$

In this case, the minima of the magnetoresistance oscillation occur when

$$\frac{2R_c}{a} = n + \frac{1}{4} \quad n = 1, 2, 3, \dots \quad (2.16)$$

Figure 2.5 shows one of the first experimental observations of the magnetic Weiss oscillation effect [10]. In this experiment, a periodic magnetic field was produced by an array of Ni strips on the surface of a 2DEG specimen. Figure 2.5-(a) shows the magnetoresistance traces in up- and down-sweep

of the external magnetic field (applied normal to the 2DEG plane). The hysteresis is due to that of the magnetization of the Ni strips. The arrows mark the expected positions of resistance minima for the magnetic Weiss oscillation. The magnetic Weiss oscillation is more clearly seen in Figure 2.5-(b), which shows the difference between the traces for the up sweep and down sweep.

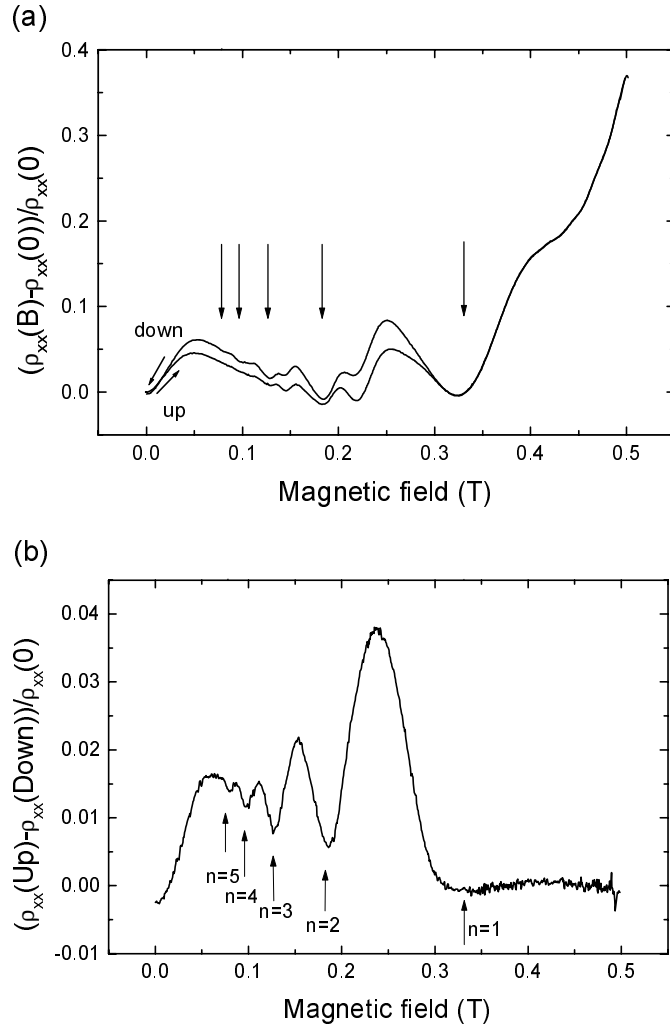


**Figure 2.5:** (a) Magnetoresistance of a device with period  $a=0.5\mu\text{m}$  at  $T=4.2\text{K}$ . The gate bias  $V_g=500\text{mV}$ . Up-sweep and down-sweep traces are shown. The hysteresis originates from that of magnetization for Ni stripes. (b) The difference between up- and down-sweeps (hysteresis component of (a)) is shown. The arrows indicated the expected positions of resistivity minima for *magnetic* Weiss oscillation (eq. (2.16))[10].

## 2.3 Coexisting electric and magnetic modulations

When the ferromagnetic stripes are magnetized by a vertical magnetic field, the resulting magnetic modulation at the 2DEG plane is in-phase with the electrostatic modulation as depicted in Fig. 2.6 (*i.e.*  $V(x) = V_0 \cos 2\pi x/a$  and  $B_z(x) = B_0 \cos 2\pi x/a$ ). The electrostatic modulation is always brought

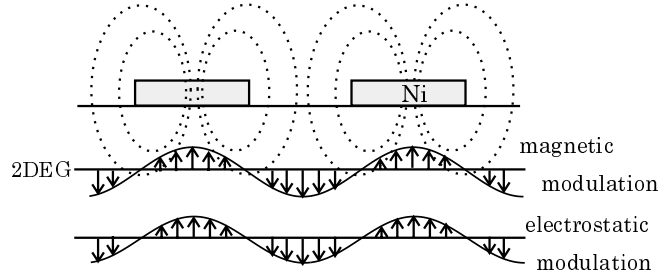


**Figure 2.6:** Schematic drawings of the 2DEG with spatially modulated magnetic field. When the ferromagnetic stripes are vertically magnetized, the resultant magnetic modulation at the 2DEG plane is in-phase with the electrostatic modulation.

about in real system, even if we do not apply bias voltage to the striped gate. An experimental obstacle encountered in the early studies of magnetic Weiss oscillation was that the microstructured metal on the surface of a 2DEG specimen produced a strain-induced potential modulation [7]. In the work cited earlier [10], a gate bias is used to counteract and cancel the strain-induced potential. Therefore, it is helpful to consider the case of "coexisting electric and magnetic modulations" in order to understand the real system.

If the two types of modulation are spatially in-phase, (*i.e.*  $V(x) = V_0 \cos 2\pi x/a$  and  $B_z(x) = B_0 \cos 2\pi x/a$ ), the conductivity takes the form

$$\sigma_{yy} \approx \frac{e^2}{\hbar} \frac{2\pi^2 \tau}{\hbar} \frac{\ell^2}{a^2} \sum_n [\hbar\omega_0 G_n(u) + V_0 F_n(u)]^2 \times \left( -\frac{\partial f(E)}{\partial E} \right)_{E=E_n}. \quad (2.17)$$

The asymptotic expression reads

$$\begin{aligned} \frac{\sigma_{yy}}{\sigma_0} &\approx \frac{ak_F}{2\pi^2} \frac{\hbar\omega_0}{\hbar\omega_c} \frac{\hbar\omega_0}{E_F} (1 + \delta^2) \left\{ 1 - A(T/T_a) \right. \\ &+ \left[ A(T/T_a) - 2e^{-\pi/\omega_c \tau_f} A(T/T_c) \cos \left( \frac{2\pi E_F}{\hbar\omega_c} \right) \right] \\ &\times \sin^2 \left( \frac{2\pi R_c}{a} - \frac{\pi}{4} + \phi \right) \left. \right\} \end{aligned} \quad (2.18)$$

where

$$\delta \equiv \frac{2\pi m^* V_0}{ak_F \hbar e B_0} = \tan \phi. \quad (2.19)$$

The parameter  $\delta$  represents the ratio of the electrostatic potential modulation amplitude  $V_0$  and the magnetic field modulation amplitude  $B_0$ . Equation (2.18) gives the oscillatory part of magnetoresistance

$$\rho_{xx} \propto (1 + \delta^2) \sin^2 \left( \frac{2\pi R_c}{a} - \frac{\pi}{4} + \phi \right). \quad (2.20)$$

We see that the Weiss oscillation pattern shifts horizontally as a function of  $\delta$ , in such a way that the positions of the resistance minima become

$$\frac{2R_c}{a} = n + \frac{1}{4} - \frac{1}{\pi} \arctan \delta \quad (n = 1, 2, 3, \dots). \quad (2.21)$$

This sort of phase shift as a function of  $\delta$  has been experimentally verified [16]. Figure 2.7-(a) shows that oscillation minima shift by changing the relative strength of the two modulations. Figure 2.7-(b) shows the comparison of the observed phase shift  $\varphi$  and the parameter  $\delta$  evaluated from the analysis of the Weiss oscillation amplitude. It is seen that the relation  $\delta = \tan \phi$  is well obeyed.

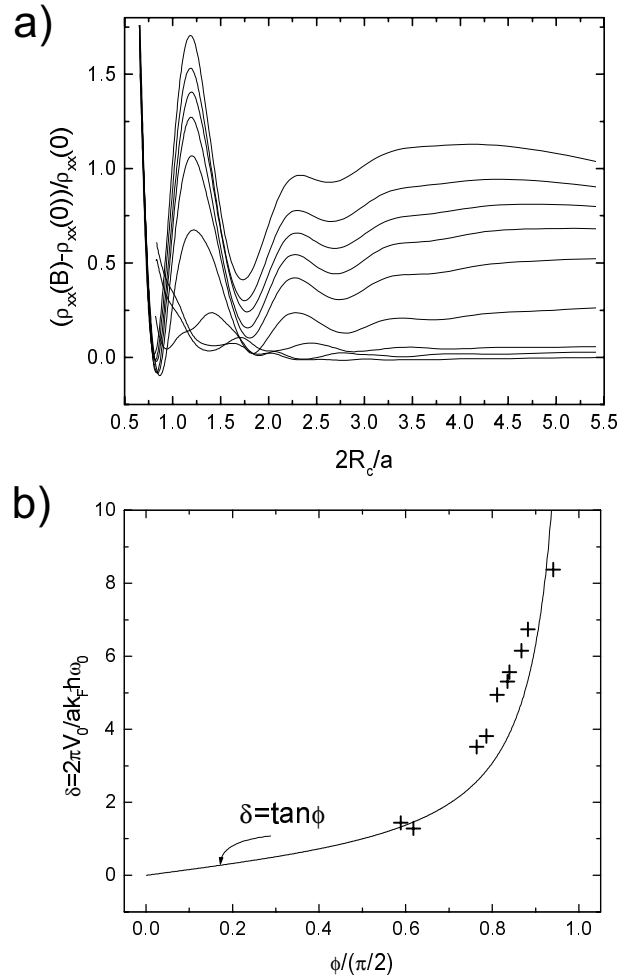


**Figure 2.7:** (a) Magnetoconductance of a device with period  $a=0.5\mu\text{m}$  at  $T=4.2\text{K}$  is plotted against  $2R_c/a$  for a different gate bias voltages;  $V_g=+500\text{mV}$  (bottom), 250, 50, -50, -110, -125, -150, -175, and -200 (top) mV. (b) The plot of relative amplitude parameter  $\delta$  versus the *phase term*  $\phi$  of the magnetoconductance oscillation. Dotted curve depicts the relation eq. (2.19) [16].



# Chapter 3

## The case of out-of-phase electric and magnetic modulations

### 3.1 Introduction

In the present work, we employ an experimental configuration in which the spatial phase relation between the electric and magnetic fields is different from what we considered thus far. If the two types of modulation are  $\pi/2$  out-of-phase (*i.e.*  $V(x) = V_0 \cos 2\pi x/a$  and  $B_z(x) = B_0 \sin 2\pi x/a$ ), the asymptotic expression for  $\sigma_{yy}$  is given by

$$\frac{\sigma_{yy}}{\sigma_0} = \frac{ak_F \hbar\omega_0 \hbar\omega_c}{2\pi^2 \hbar\omega_c E_F} \left\{ G + \delta^2 F - 2e^{-\pi/\omega_c\tau_f} A(T/T_c) \cos\left(\frac{2\pi E_F}{\hbar\omega_c}\right) D \right\}, \quad (3.1)$$

where

$$D = \delta^2 - (\delta^2 - 1) \sin^2\left(\frac{2\pi R_c}{a} - \frac{\pi}{4}\right).$$

In contrast to the in-phase case (eq. (2.18)), the parameter  $\delta$  is not contained in the argument of the  $\sin^2$ -term. In this case, therefore, the Weiss oscillation pattern is inverted without any phase shift, as the value of  $\delta$  is varied from  $\delta \gg 1$  to  $\delta \ll 1$ .

### 3.2 Experimental system

Samples used in the present study were fabricated from a GaAs/AlGaAs single heterojunction wafer grown by molecular beam epitaxy (MBE). The

structure of the sample wafer is shown in Fig. 3.1. The 2DEG in the wafer

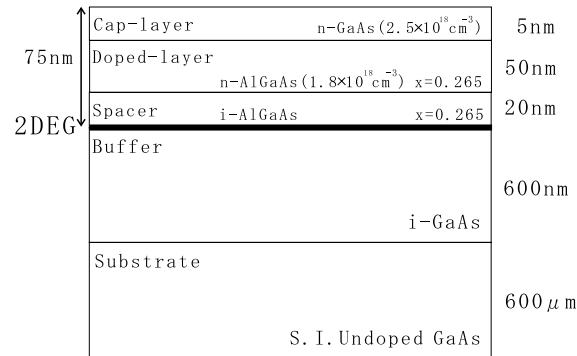


**Figure 3.1:** The structure of a GaAs/AlGaAs single heterojunction wafer.

had the density  $n_e = 2.0 \times 10^{15} \text{ m}^{-2}$  and mobility  $\mu = 60 \text{ m}^2 \text{ V}^{-1} \text{ s}^{-1}$  at 1.5 K. We can increase the density  $n_e$  by illuminating with an LED mounted above the sample. This effect is known as "persistent photo conductivity effect". The depth of the heterointerface from the surface was 75 nm. A standard Hall-bar pattern was defined by photolithography and wet etching. An array of 60 nm thick ferromagnetic (Ni or Co) strips with periodicity  $a$  ( $a/2$  wide and  $a/2$  apart) was fabricated on the surface by electron-beam lithography, vacuum deposition and lift-off process. The ferromagnetic stripes were all connected so that a gate bias could be applied to them. All the samples used in our experiment had periodicity  $a = 500 \text{ nm}$  (see Fig. 3.2). Recently, it has been shown that the strain-induced potential is mostly due to the piezoelectric coupling, and that it can be minimized by setting the direction of modulation parallel to the [100] crystallographic direction [11, 14, 12]. Accordingly, we patterned the Hall-bar with the current direction aligned to the [100] axis.

Transport measurements were carried out using a standard low-frequency ac technique. The capability of precisely aligning the magnetic field direction with respect to the 2DEG plane and to the stripe pattern was important. The cross-coil magnet system used in the present work consisted of a 6T split-coil superconducting magnet in combination with a small homemade solenoid. It enabled us to independently control the horizontal and vertical components of the magnetic field (Fig. 3.3).

A rotating sample holder sketched in Fig. 3.4, was used to adjust the angle

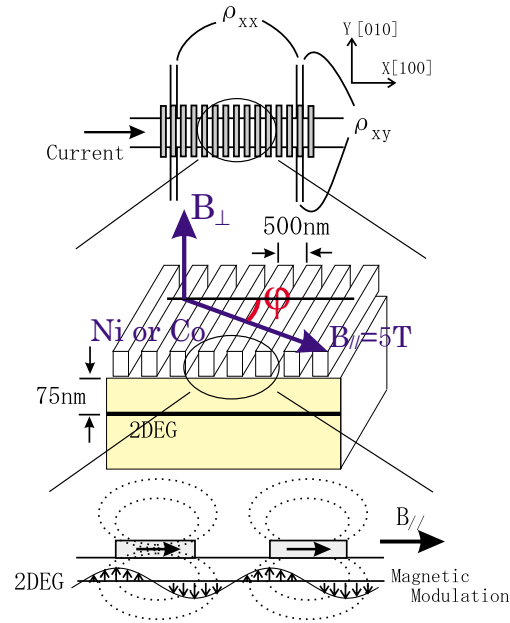


**Figure 3.2:** The structure of the sample with the modulation wavevector parallel to the current channel. Definition of azimuthal angle  $\varphi$  is also shown. When the ferromagnetic stripes are horizontally magnetized, the resultant magnetic modulation at the 2DEG plane exists.

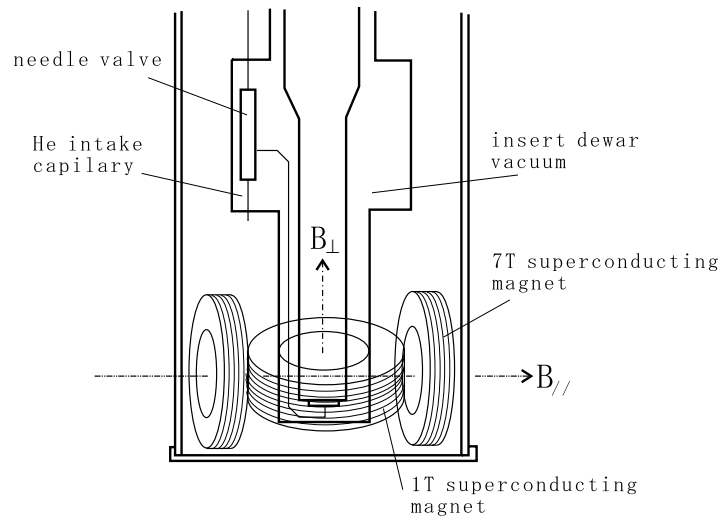


**Figure 3.3:** Schematic diagram of cross-coil magnet system. The magnet system consisted of a 7T split-coil superconducting magnet in combination with a 1T small homemade solenoid. It enabled us to independently control the horizontal and vertical components of the magnetic field.

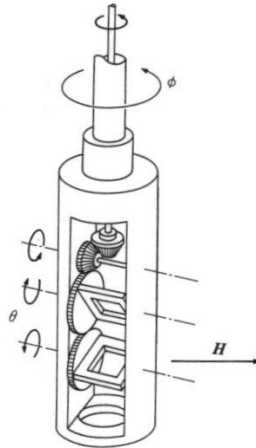


**Figure 3.4:** Schematic diagram of rotating sample holder. The azimuthal angle  $\varphi$  was varied by turning the sample holder about its vertical axis. For each setting of  $\varphi$ , the horizontal alignment was readjusted by rotating the sample stage at an angle  $\theta$ .

of the sample-mounting stage so as to make the 2DEG plane horizontal. The azimuthal angle  $\varphi$  between the horizontal magnetic field and the direction of the modulation was varied by turning the sample holder about its vertical axis. For each setting of  $\varphi$ , the horizontal alignment was readjusted. The misalignment component that was not accessible by the sample rotation stage was compensated by putting a small offset of the vertical field.

The horizontal magnetic field served to control the magnetization of the ferromagnetic gate, and the vertical field was used for measurements of magnetotransport in the 2DEG. This scheme allowed us to keep the ferromagnetic strips fully polarized while working with low (or even zero) perpendicular field for the 2DEG.

### 3.3 The control of magnetic field modulation

When the ferromagnetic strips are magnetized by the horizontal magnetic field, the resulting magnetic field modulation at the 2DEG plane is expected to be out-of-phase with the electrostatic modulation as shown in Fig. 3.5 (*i.e.*  $V(x) = V_0 \cos 2\pi x/a$  and  $B_z(x) = B_0 \sin 2\pi x/a$ ).

This is seen in Fig. 3.6, which shows the magnetoresistance as a function

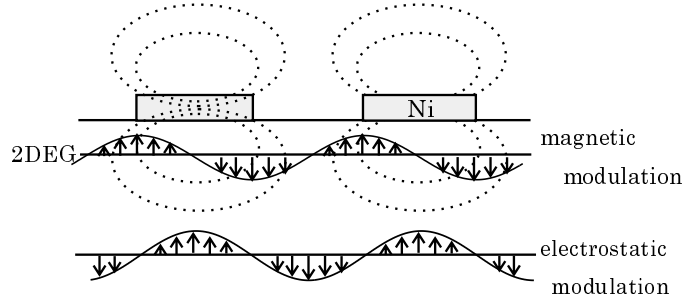


**Figure 3.5:** Schematic drawings of the 2DEG with spatially modulated magnetic field. When the ferromagnetic stripes are horizontally magnetized, the magnetic and electrostatic modulations are out-of-phase.

of the perpendicular magnetic field  $B_{\perp}$  with zero gate bias and under a constant parallel field  $B_{\parallel} = 5$  T at  $T=1.5$ K. This parallel magnetic field is much higher than the saturation field  $B \approx 0.3$  T for nickel, so that the magnetization of the nickel stripes are fixed irrespective of the change in  $B_{\perp}$ . The different traces are taken with the parallel field applied at different azimuthal angles  $\varphi$ . The oscillations observed in the field range  $B_{\perp} < 0.3$  T are the Weiss oscillations, while the shorter period oscillations at higher  $B_{\perp}$  are the Shubnikov-de Haas effect. No hysteresis appears because the magnetization of the nickel strips is fixed by the constant horizontal field  $B_{\parallel} = 5$  T. Note that only the magnetization component parallel to the modulation direction is effective in generating the magnetic field modulation at the 2DEG plane.

Figure 3.7 is a replot of the data in Fig. 3.6 as a function of  $2R_c/a$  calculated by using the value of  $n_e$  as determined from the Shubnikov-de Haas effect. The traces for  $\varphi \leq 60^\circ$  have their minima at the positions in agreement with eq. (2.16) (vertical dotted lines in the figure). However, the minima turn to maxim in traces for higher values of  $\varphi$ , namely the Weiss oscillation diminishes in amplitude with increasing  $\varphi$  and is eventually inverted without any phase shift. This peak/valley inversion corresponds to the behavior expected for the case of the out-of-phase electrostatic and magnetic modulations.

We can evaluate the modulation amplitude by fitting the Weiss oscillation with the theoretical formula given by eq. (3.1). Let us begin with the case  $\varphi = 90^\circ$ . For this field orientation, the nickel stripes are magnetized along their length so that the magnetic field modulation produced at the 2DEG

plane is minimal. The Weiss oscillation observed in this configuration is mostly due to the strain-induced electrostatic modulation. The amplitude of the strain-induced electrostatic modulation extracted from this data is  $V_0 = 0.10$  meV, which is much smaller than  $V_0 \sim 1.0$  meV when we patterned the current direction aligned to [110] direction. By using the determined value  $V_0$ , the values of  $B_0$  for different  $\varphi$  settings can be extracted from these data. The results are plotted in Fig. 3.8 for the sample with Ni or Co striped gate, which clearly shows the expected  $\cos \varphi$  dependence. The  $\cos \varphi$  dependence shows that only the component of magnetization of ferromagnetic strips parallel to the current is relevant to the amplitude of magnetic field modulation  $B_0$ . The maximum amplitude of the magnetic field modulation at the 2DEG plane in these samples are found to be  $B_0 = 19.1$  mT for Ni and  $B_0 = 52$  mT for Co.

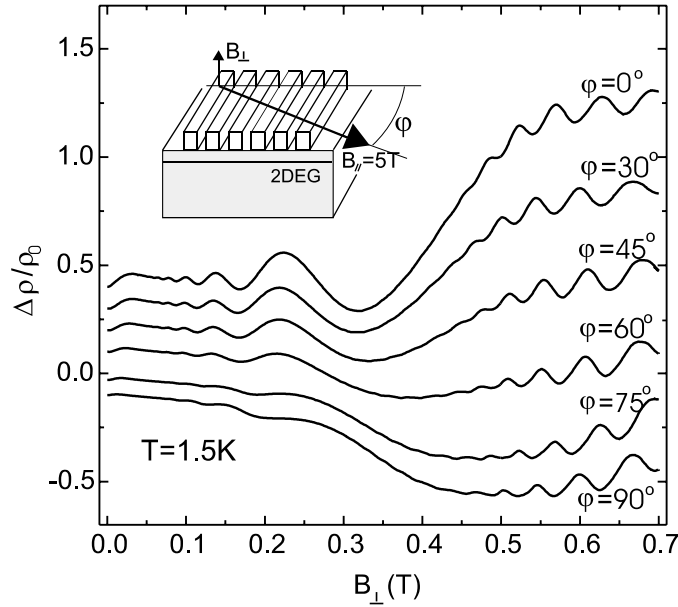


**Figure 3.6:** Magnetoresistance of the device with Ni striped gate at  $T=1.5K$  for different settings of azimuthal angle  $\varphi$  of the parallel magnetic field defined as shown in the inset. The value of  $\varphi$  is (from top to bottom)  $0^\circ$ ,  $30^\circ$ ,  $45^\circ$ ,  $60^\circ$ ,  $75^\circ$  and  $90^\circ$ . The traces are vertically shifted for clarity.

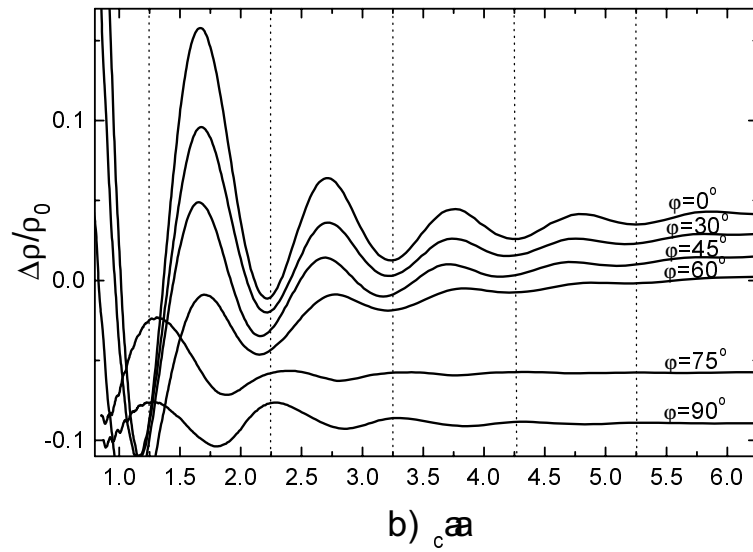


**Figure 3.7:** The data shown in Fig. 3.6 replotted as a function of  $2R_c/a$  at  $T=1.5\text{K}$ . The values of  $\varphi$  are (from top to bottom)  $0^\circ$ ,  $30^\circ$ ,  $45^\circ$ ,  $60^\circ$ ,  $75^\circ$  and  $90^\circ$ . The traces are vertically shifted for clarity.

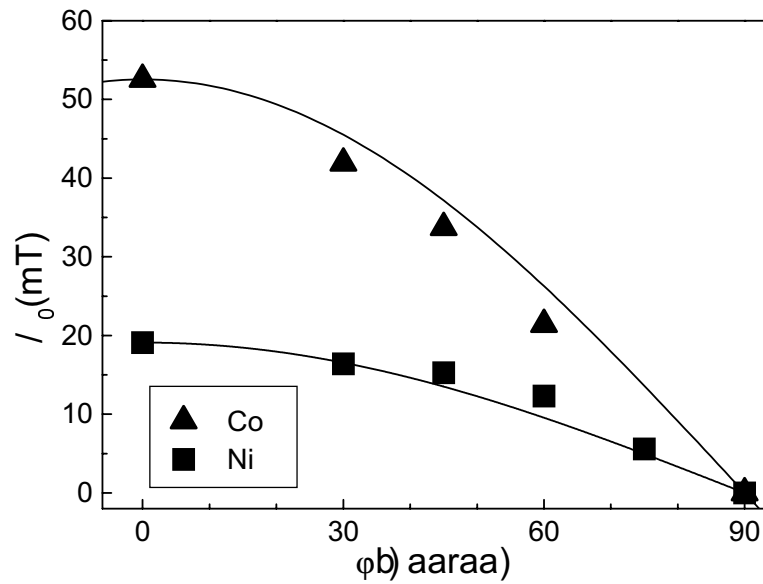


**Figure 3.8:** The  $\cos\varphi$ -dependence of the amplitude  $B_0$  of magnetic field modulation at the 2DEG plane for the samples with Ni or Co ferromagnetic striped gate.

### 3.4 The control of electric field modulation

The peak-valley inversion of Weiss oscillation can be also achieved by changing the gate bias. Figure 3.9 shows the magnetoresistance traces for different values of gate bias  $V_g$  ranging from -200mV to 200mV. Figure 3.10 is a replot of the data in Fig. 3.9 as a function of  $2R_c/a$ . For this series of measurements, the magnetic modulation is fixed at  $B = 12$  mT by setting  $B_{\parallel} = 5$  T at  $\varphi = 55^\circ$ . The amplitude  $V_0$  of the electrostatic potential modulation as determined from the analysis of the Weiss oscillation amplitude is plotted as a function of the applied gate bias  $V_g$  in Fig. 3.11. The electrostatic modulation amplitude in the present system can be approximately written as  $V_0 \approx -1.2 \times 10^{-3} V_g + 0.10$  mV. The first term represents the gate-bias-induced component which is roughly proportional to  $V_g$ . The coefficient  $1.2 \times 10^{-3}$  is the reduction factor which depends on the distance of the 2DEG from the patterned gate and on the details of screening. The value  $V_0 = 0.10$  meV at  $V_g = 0$  represents the strain-induced component. It is noted that the strain-induced component in the present sample is about an order of magnitude smaller than those for samples with the modulation structure made along the [110] direction [16]. Since the strain-induced potential due to the piezoelectric coupling is minimized in the present system, the one that plays the role here may be attributed to deformation potential coupling [14].

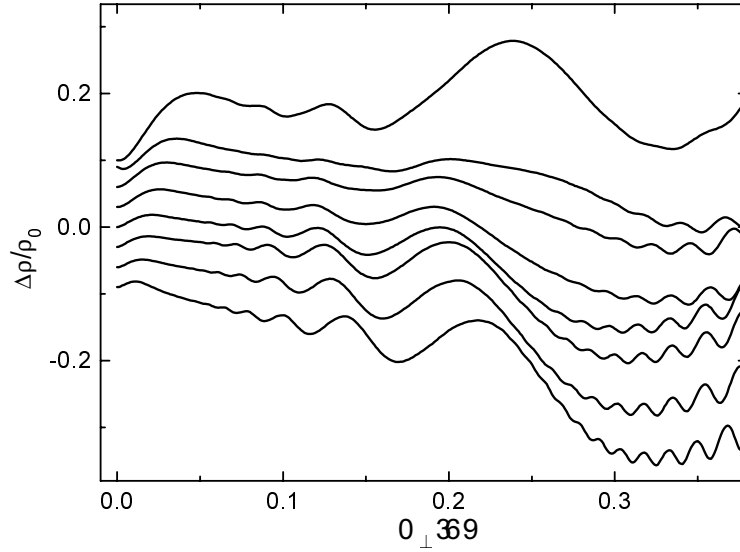


**Figure 3.9:** Magnetoresistance of the device with Ni striped gate for different values of the gate bias  $V_g$  with the magnetic modulation amplitude fixed at  $B_0 = 12$  mT by setting  $B_{\parallel} = 5T$  at  $\varphi = 55^\circ$  at  $T=1.5K$ . The values of  $V_g$  are (from top to bottom) -200, -100, -80, -50, 0, 50, 100, and 200 mV. The traces are vertically shifted for clarity.

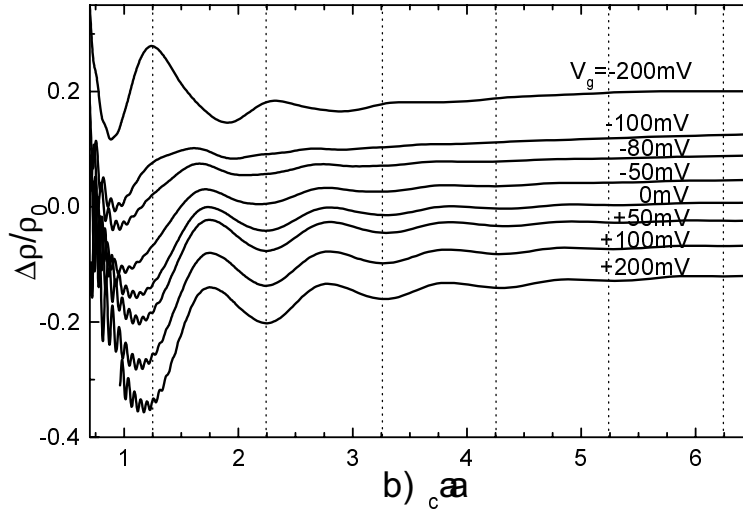


**Figure 3.10:** The data shown in Fig. 3.9 replotted as a function of  $2R_c/a$  at  $T=1.5K$ . The magnetic modulation amplitude is fixed at  $B_0 = 12$  mT. The values of  $V_g$  are (from top to bottom) -200, -100, -80, -50, 0, 50, 100, and 200 mV. The traces are vertically shifted for clarity.

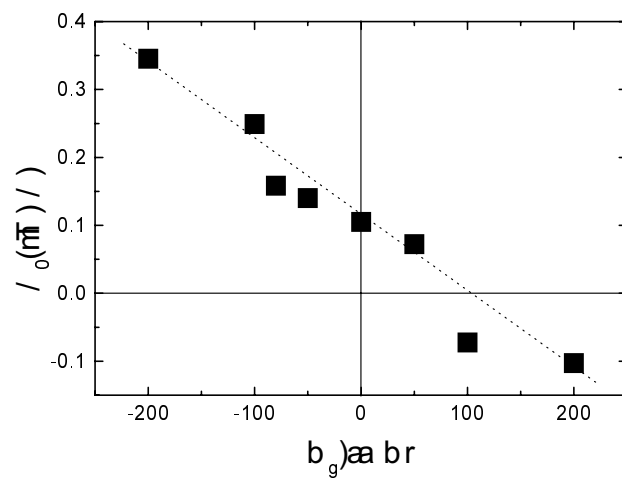


**Figure 3.11:** The change in the electrostatic potential modulation amplitude  $V_0$  as a function of  $V_g$ . The  $V_0$  at  $V_g = 0$  represents the strain-induced component.

# References

- [1] D. Weiss, K. von Klitzing, K. Ploog, and G. Weimann, *Europhys. Lett.* **8**, 179 (1989).
- [2] R.R. Gerhardts, D. Weiss, and K. von Klitzing, *Phys. Rev. Lett.* **62**, 1173 (1989).
- [3] R.W. Winkler, J.P. Kotthaus, and K. Ploog, *Phys. Rev. Lett.* **62**, 1177 (1989).
- [4] C.W.J. Beenakker, *Phys. Rev. Lett.* **62** 2020 (1989).
- [5] F.M. Peeters and P. Vasilopoulos, *Phys. Rev.* **B46**, 4667 (1992).
- [6] D. Yoshioka and Y. Iye, *J. Phys. Soc. Japan* **56** 448 (1987).
- [7] R. Yagi and Y. Iye, *J. Phys. Soc. Jpn.* **62**, 1279 (1993).
- [8] D.P. Xue and G. Xiao, *Phys. Rev. B* **45**, 5986 (1992).
- [9] F.M. Peeters and P. Vasilopoulos, *Phys. Rev.* **B47**, 1466 (1993).
- [10] S. Izawa, S. Katsumoto, A. Endo, and Y. Iye, *J. Phys. Soc. Jpn.* **64**, 706 (1995).
- [11] P.D. Ye, D. Weiss, R.R. Gerhardts, M. Seeger, K. von Klitzing, K. Eberl, and H. Nickel, *Phys. Rev. Lett.* **74**, 3013 (1995).
- [12] H.A. Carmona, A.K. Geim, A. Nogaret, P.C. Main, T.J. Foster, M. Henini, S.P. Beaumont, and M.G. Blamire, *Phys. Rev. Lett.* **74**, 3009 (1995).
- [13] E. Skuras, A.R. Long, I.A. Larkin, J.H. Davies, and M.C. Holland, *Appl. Phys. Lett.* **70** 871 (1997).

- [14] J.H. Davies and I.A. Larkin: Phys. Rev. **B49** 4800 (1994); I.A. Larkin, J.H. Davies, A.R. Long and R. Cusco: Phys. Rev. **B56** 15242 (1997)
- [15] A. Nogaret, S. Carlton, B.L. Gallagher, P.C. Main, M. Henini, R. Wirtz, R. Newbury, M.A. Howson, and S.P. Beaumont, Phys. Rev. **B55** 16037 (1997).
- [16] A. Endo, S. Izawa, S. Katsumoto and Y. Iye: Surf. Sci. **361/362** 333 (1996).

# Chapter 4

## Electron-electron umklapp process in 2DEG under a spatially alternating magnetic field

### 4.1 Introduction

Electron-electron interaction is one of the most essential processes in condensed matter physics. It is essential for the energy relaxation within an electron system. However, its role in the momentum relaxation is rather subtle. It cannot contribute to resistivity in a Galilean invariant system having continuous translational symmetry, because the total momentum of two colliding electrons is conserved there. It is only with the participation of a crystal lattice, *i.e.* the Umklapp process, that momentum relaxation occurs

---

The content of this chapter was reported in M. Kato, A. Endo and Y. Iye: Phys. Rev. **B58** 4876 (1998); M. Kato, A. Endo and Y. Iye: J. Phys. Soc. Jpn. **68** 1492 (1999); M. Kato, A. Endo, S. Katsumoto and Y. Iye: J. Phys. Soc. Japan **68** No.8 2870 (1999); M. Kato, A. Endo, S. Katsumoto and Y. Iye: Proc. of the 6th International Symposium on Foundations of Quantum Mechanics in the Light of New Technology (ISQM-Tokyo'98), (A.R.L., Hitachi Ltd., Hatoyama, Saitama, Japan, Aug., 1998), in press; M. Kato, A. Endo, S. Katsumoto and Y. Iye: Proc. of the 13th Int. Conf. on the Electronic Properties of Two-Dimensional Systems (EP2DS-13), (Ottawa, Aug., 1999), in press.

by electron-electron scattering[1]. When it does occur, the electron-electron Umklapp scattering generally gives rise to a  $T^2$ -dependent resistivity. Such a  $T^2$ -term in resistivity has been observed in alkali metals, and is very conspicuous in so-called strongly correlated electron systems such as heavy fermion metals, transition metal oxides and organic conductors. Although there has been much progress in the theoretical understanding of the issue [2–4], a truly quantitative comparison between theory and experiment seems difficult at the moment, because a full treatment of the relevant electron-electron process requires detailed knowledge of the complex band structure of real materials and the Umklapp matrix element. It is desirable, thus, to find a simplest possible experimental system that exhibits the phenomenon at issue.

In the previous chapter, we have demonstrated that spatially modulated magnetic field  $B_z(x) = B_0 \cos Kx$  can be imposed on the 2DEG at the GaAs/AlGaAs heterointerface, and that the modulation amplitude can be precisely determined from analysis of the Weiss oscillation. The present system allows us to break the translational symmetry in a controlled fashion, so that it may provide an excellent test ground for this problem. This issue is recently addressed by Messica *et al.* [5] for electrostatic modulation. They have measured the low temperature resistance of 2DEG for different gate bias settings and found an excess resistance with a quadratic temperature dependence, which is taken as a signature of the electron-electron scattering. In this work, we use magnetic field modulation as the artificial periodicity. There is a good reason for the preference of the magnetic over the electrostatic modulation. Namely, use of magnetic modulation has a distinct advantage that it allows us to change the modulation amplitude without affecting the density of 2DEG. This is a crucial point in addressing the issue of the electron-electron scattering, because the electron-electron interaction is anticipated to be sensitive to the electron density.

## 4.2 Theory -Temperature dependence of electron lifetime-

Consider first, two colliding electrons as shown in Fig. 4.1. An electron in state  $\mathbf{k}_1$  is scattered into state  $\mathbf{k}'_1$  with a change in energy by  $E(\mathbf{k}'_1) - E(\mathbf{k}_1)$ . Another electron in state  $\mathbf{k}_2$  is scattered into state  $\mathbf{k}'_2$  with a change in

energy by  $E(\mathbf{k}'_2) - E(\mathbf{k}_2)$  at the same time. All the four electron states lie within the thermal layer, of width  $\sim k_B T$ , that straddles the Fermi surface. Conservation of energy requires

$$E(\mathbf{k}_1) + E(\mathbf{k}_2) = E(\mathbf{k}'_1) + E(\mathbf{k}'_2). \quad (4.1)$$

Similarly, conservation of momentum requires

$$\mathbf{k}_1 + \mathbf{k}_2 = \mathbf{k}'_1 + \mathbf{k}'_2. \quad (4.2)$$

The scattering rate of the electron in state  $\mathbf{k}_1$  is given by

$$1/\tau_{e-e}(\mathbf{k}_1) = \sum_{\mathbf{k}_2, \mathbf{k}'_1, \mathbf{k}'_2} P(\mathbf{k}_1, \mathbf{k}_2; \mathbf{k}'_1, \mathbf{k}'_2) \quad (4.3)$$

where  $P(\mathbf{k}_1, \mathbf{k}_2; \mathbf{k}'_1, \mathbf{k}'_2)$  is the probability that an electron in state  $\mathbf{k}_1$  is scattered into state  $\mathbf{k}'_1$  while another electron in state  $\mathbf{k}_2$  is scattered into state  $\mathbf{k}'_2$ , while obeying eq. (4.1) and eq. (4.2). In three dimensional case,

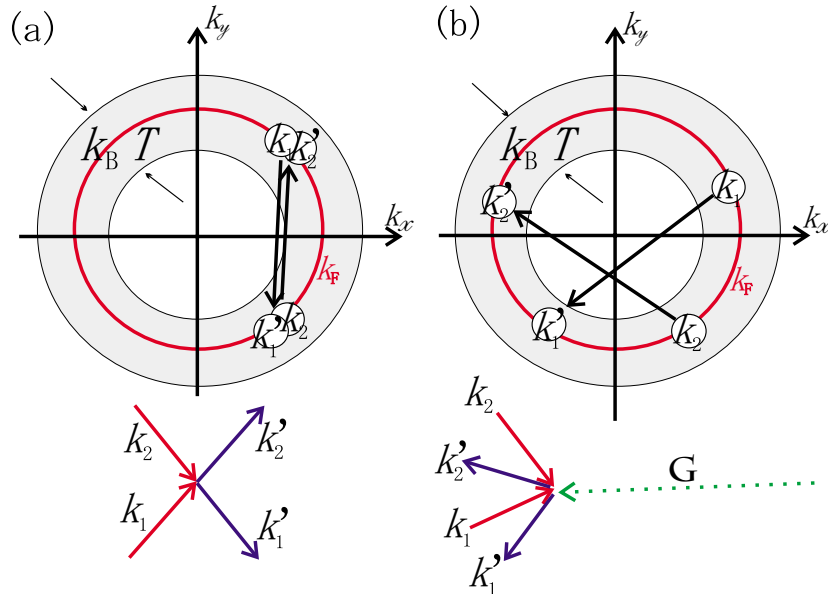


**Figure 4.1:** Schematic diagram of (a)normal and (b) umklapp electron-electron scattering. The thermal layer of width  $k_B T$  is shown by the shaded area straddling the Fermi surface.

we have a sum over nine variables ( $\mathbf{k}_2, \mathbf{k}'_1, \mathbf{k}'_2$ ) since  $\mathbf{k}_1$  is fixed. However, only five of these variables are independent as eq. (4.1) and eq. (4.2) give

us four constraints. If we may choose the five independent variables as  $\mathbf{q} = \mathbf{k}'_1 - \mathbf{k}_2$ ,  $E(\mathbf{k}_2)$  and  $E(\mathbf{k}'_1)$ , eq. (4.3) can be written as

$$1/\tau_{e-e}(\mathbf{k}_1) = \sum_{\mathbf{q}, E(\mathbf{k}_2), E(\mathbf{k}'_1)} P(\mathbf{q}, E(\mathbf{k}_2), E(\mathbf{k}'_1)). \quad (4.4)$$

The number of states in  $\mathbf{k}$ -space available for scattering with energies  $E(\mathbf{k}_2)$  and  $E(\mathbf{k}'_1)$  is proportional to  $k_B T/E_F$  for each independent variable. This leads

$$1/\tau_{e-e} \propto T^2, \quad d = 3. \quad (4.5)$$

As mentioned before, electron-electron scattering comes to contribute to the resistivity by umklapp process. It is noted that umklapp process will not change the above temperature dependence of the electron lifetime but only its magnitude. The above argument also gives the result

$$1/\tau_{e-e} \propto T, \quad d = 1 \quad (4.6)$$

for one dimensional case. Finally, let us consider the results for the two dimensional case. Is it  $T^2$  or  $T$ ? We cannot apply the above arguments directly to obtain the result for two dimensional case. A detailed calculation of  $\tau_{e-e}$  in two dimensions was given by Giuliani and Quinn [7] to yield

$$1/\tau_{e-e} \propto T^2 \ln(E_F/k_B T), \quad d = 2. \quad (4.7)$$

Note that the situation in a real system is even more complicated than indicated by eq. (4.7). We will see the comparison between the theory and our experimental results in Section 4.4.

### 4.3 The observation of $T^2$ -dependence of resistivity

Figure 4.2 shows the resistivity of a GaAs/AlGaAs 2DEG with a striped Ni gate (the same sample as the one shown in Fig. 3.6 to Fig. 3.11) as a function of the parallel magnetic field  $B_{\parallel}$  with  $B_{\perp} = 0$  at  $T=1.3\text{K}$ . Two traces correspond to  $\varphi = 0^\circ$  ( $B_0 = 19.1 \text{ mT}$ ) and  $90^\circ$  ( $B_0 = 0$ ), respectively. Note that the magnetic field is aligned exactly parallel to the 2DEG plane, so that there is no uniform perpendicular field component. For  $\varphi = 90^\circ$ , the

resistivity is found to be independent of the applied magnetic field except for a small peak in the low field region where the magnetization reversal occurs. As mentioned in Section 3.3, the magnetic field modulation vanishes for this field orientation, so that the observed field-independent resistivity can be taken as the reference value for zero modulation amplitude. The origin of the small peak can be interpreted as follows. During the magnetization reversal, small domains with different magnetization directions are formed, and they produce a certain degree of magnetic field nonuniformity at the 2DEG plane which contributes to the carrier scattering. For  $\varphi = 0^\circ$  at which the magnetic modulation is maximum, a resistance change by about 5% is observed. The constant resistivity for  $B > 0.3$  T gives the value under the maximum magnetic field modulation  $B_0 = 19.1$  mT as determined from the Weiss oscillation. We define the excess resistivity  $\Delta\rho$  by the difference between the values for the two field orientations, as indicated in the figure.

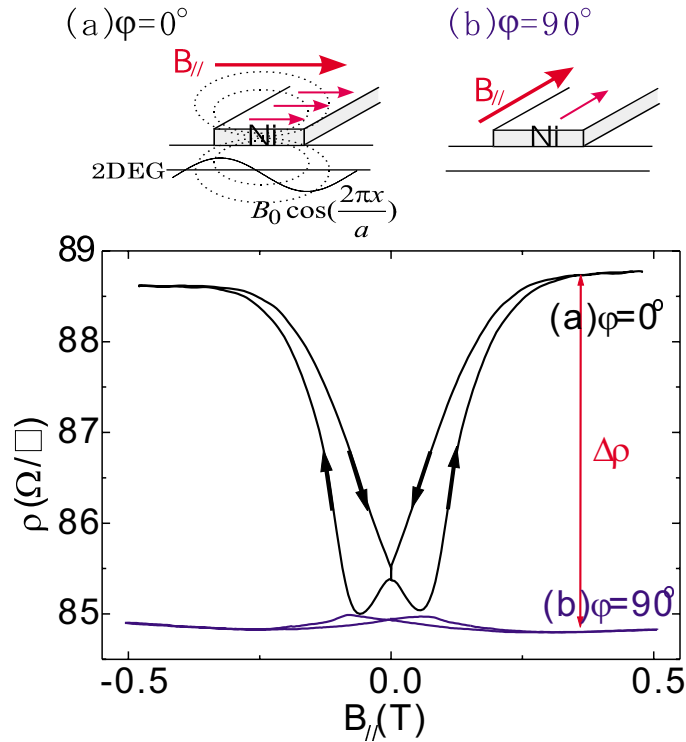


**Figure 4.2:** Resistivity as a function of  $B_{\parallel}$ , with  $B_{\perp} = 0$ . The two traces correspond to (a)  $\varphi = 0^\circ$  ( $B_0 = 19.1$  mT) and (b)  $90^\circ$  ( $B_0 = 0$ ) at  $T=1.3$ K. The excess resistivity  $\Delta\rho$  is defined by the difference between the values for the two field orientations.

Figure 4.3 shows the  $\varphi$  dependence of the excess resistivity  $\Delta\rho$  at  $T=1.3$ K.

As seen earlier in Fig. 3.8, the amplitude of magnetic field modulation changes as  $B_0 \propto \cos \varphi$ . Since the excess resistivity associated with the modulation should be proportional to the square of the transition matrix element,  $\Delta\rho \propto B_0^2 \propto \cos^2 \varphi$  is expected. The data shown here corroborate this dependence as demonstrated by the good fit of the  $\cos^2 \varphi$  curve.

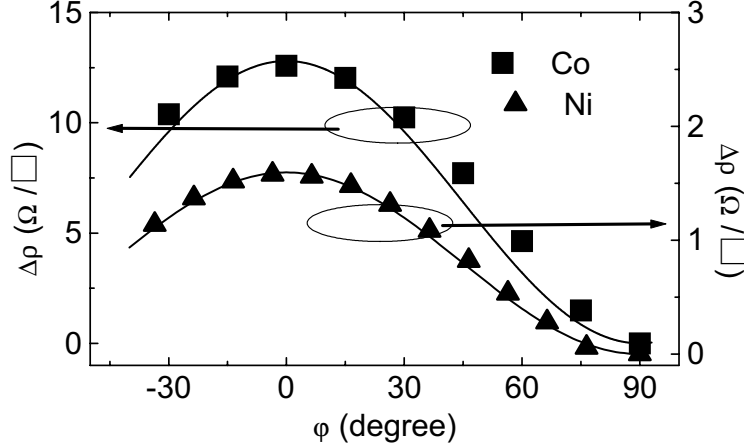


**Figure 4.3:** The excess resistivity  $\Delta\rho$  as a function of the azimuthal angle  $\varphi$  of the parallel magnetic field at  $T=1.3\text{K}$ . The observed  $\cos^2 \varphi$  dependence (solid line) verifies the relation  $\Delta\rho \propto B_0^2$ .

Figure 4.4(a) shows the temperature dependence of resistivity for  $\varphi = 0^\circ$  ( $B_0 = 52 \text{ mT}$ ) and for  $\varphi = 90^\circ$  ( $B_0 = 0$ ). The resistivity for the latter case is basically the same as that of the plain 2DEG, and is written for  $T < 40\text{K}$  as

$$\rho_0(T) = \frac{m^*}{n_e e^2 \tau_{total}} = \frac{m^*}{n_e e^2} \left( \frac{1}{\tau_0} + \frac{1}{\tau_{ph}(T)} \right)$$

$$\frac{1}{\tau_0} = \text{const}, \quad \frac{1}{\tau_{ph}(T)} = \alpha_{ph} T. \quad (4.8)$$

Here,  $1/\tau_0$  is the temperature-independent inverse scattering time limited by the elastic scattering due to impurities and the  $T$ -linear term is attributed to acoustic phonon scattering with deformation potential coupling. For  $T < 40\text{K}$ ,  $1/\tau_{total} = 5.5 \times 10^{10} + 5.8 \times 10^8 T [\text{sec}^{-1}]$  for this sample, and  $\alpha_{ph} = 3.2 \times 10^{-4} \text{Vs/m}^2\text{K}$ , which is in agreement with those reported earlier for plain 2DEG samples with similar density and mobility [8, 9].

Application of a spatially alternating magnetic field increases the resistivity by  $\Delta\rho$ . The temperature dependence of the excess resistivity  $\Delta\rho \equiv \rho(B_0 = 52\text{mT}) - \rho(B_0 = 0)$  is shown in Fig. 4.4(b).

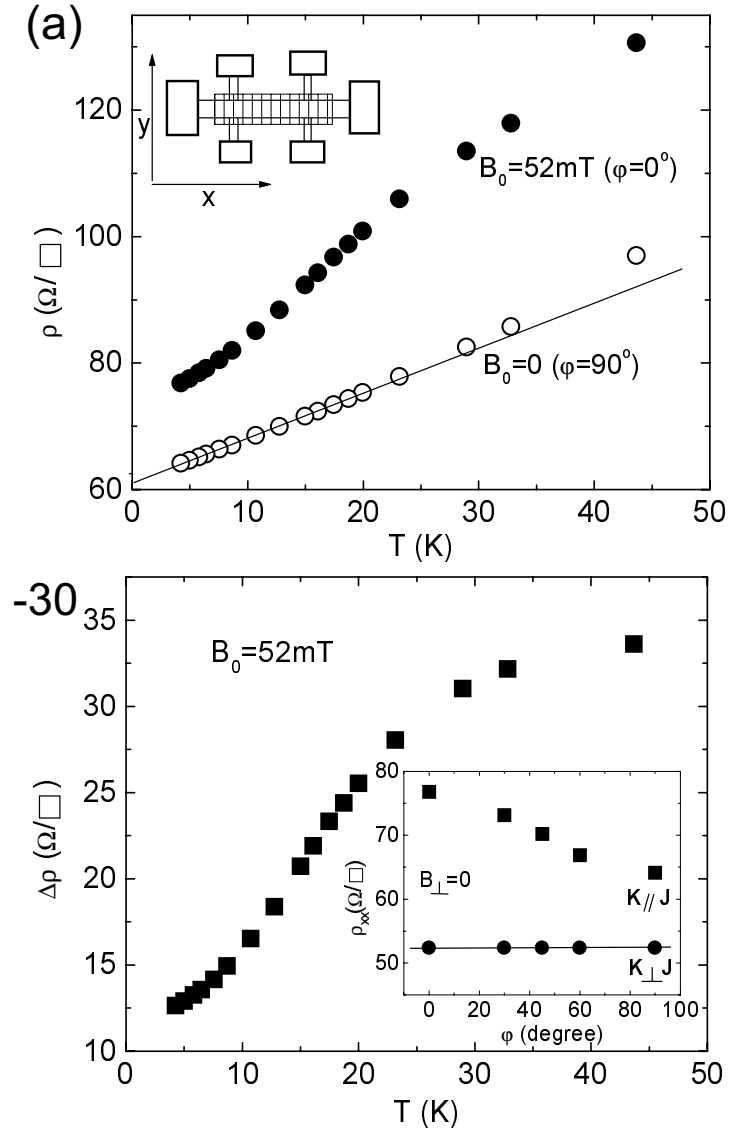


**Figure 4.4:** (a) The inset shows the structure of the sample with the modulation wave vector parallel to the current channel: ( $\mathbf{K} \parallel \mathbf{J}$ ) sample. The main panel shows the temperature dependence of resistivity under maximum magnetic modulation ( $\varphi = 0^\circ$ : solid circles) and no modulation ( $\varphi = 90^\circ$ : open circles). (b) Temperature dependence of the excess resistivity  $\Delta\rho$ . The inset shows comparison of the effect of magnetostatic modulation on resistivity between the ( $\mathbf{K} \parallel \mathbf{J}$ ) sample and the ( $\mathbf{K} \perp \mathbf{J}$ ) sample at  $T = 1.3\text{K}$

Similar measurements were carried out on a different sample with  $\mathbf{K} \perp$

$\mathbf{J}$ , in which the modulation vector  $\mathbf{K}$  is perpendicular to the direction of transport current  $\mathbf{J}$ . The solid circles in the inset of Fig. 4.4(b) indicate the total absence of the resistivity change in the  $(\mathbf{K} \perp \mathbf{J})$  sample, while the solid squares show the  $\cos^2 \varphi$ - (or,  $B_0^2$ -) dependence of  $\Delta\rho$  in the  $(\mathbf{K} \parallel \mathbf{J})$  sample. The fact that the effect vanishes when the modulation wave vector is perpendicular to the direction of transport current indicates that the effect is due to Umklapp backscattering by the periodic structure, and that a possible contribution from lithographical irregularity is of minor importance. Figure 4.5 shows the excess resistivity  $\Delta\rho$  plotted against  $T^2$  for several values

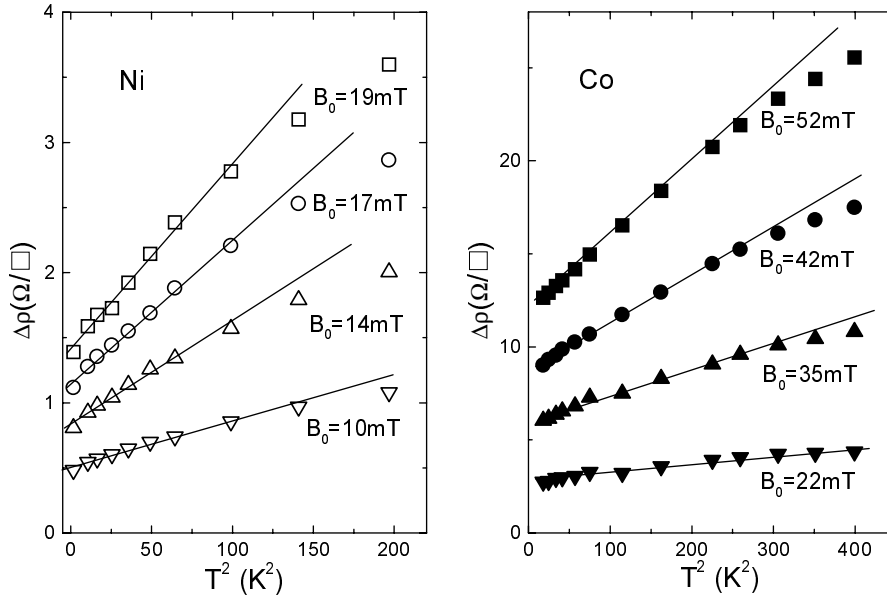


**Figure 4.5:** The excess resistivity  $\Delta\rho$  plotted against  $T^2$  for four different values of  $\varphi$ , which set the magnetic modulation amplitude, Left panel;  $B_0 = 19, 17, 14,$  and  $10$  mT for Ni stripes, and Right panel;  $B_0 = 52, 42, 35,$  and  $22$  mT for Co stripes, respectively.

of modulation amplitude  $B_0$ . These data were taken at several different settings of  $\varphi$ , which give different values of  $B_0$ , as mentioned above. It is seen that  $\Delta\rho$  at low temperatures ( $T < 20\text{K}$ ) can be expressed as  $\Delta\rho = AT^2 + C$ . The  $T^2$  term represents the electron-electron scattering, which comes to contribute to momentum relaxation in the presence of the periodic magnetic field modulation.

## 4.4 The electron density dependence of e-e scattering

In Section 4.3, we found that the excess resistivity varies as  $\Delta\rho = AT^2 + C$ , and is proportional to the square of the amplitude  $B_0$  of the alternating magnetic field. In this section, we compare our experimental results with the theoretical formula by T. Sasaki and H. Fukuyama [10]. They calculated the conductivity of 2DEG under a spatially modulated magnetic field.

Here, we consider a 2DEG subjected to a magnetic field modulation  $\mathbf{B}=(B_0 \cos Kx)\hat{z}$ . We write a Hamiltonian which includes the impurity potential  $U_{imp}$  and the electron-electron interaction  $U_{e-e}$  as

$$\begin{aligned} H &= \frac{(P - eA)^2}{2m^*} + U_{imp} + U_{e-e} \\ &= \frac{P^2}{2m^*} + U_{imp} + U_{e-e} + (\omega_0/K)p_y \sin Kx \\ &\quad + (m^*\omega_0^2/4K^2)(1 - \cos 2Kx) \end{aligned} \quad (4.9)$$

where  $\omega_0 = eB_0/m^*$ . For small values of the modulation amplitude  $B_0$ , the contribution of the term  $(m^*\omega_0^2/4K^2)(1 - \cos 2Kx) \propto B_0^2$  can be neglected. We define  $H = H_0 + H'$

$$H_0 = \frac{P^2}{2m^*} + U_{imp} \quad (4.10)$$

$$H' = U_{e-e} + (\omega_0/K)p_y \sin Kx \quad (4.11)$$

and treat  $H'$  as perturbation. Equation (4.10) can be written as

$$H_0 = \sum_k (\varepsilon_k - \mu)n_k = \sum_k (\varepsilon_k - \mu)a_k^+ a_k \quad , \varepsilon_k = \frac{\hbar^2 k^2}{2m^*}. \quad (4.12)$$

The first term of eq. (4.11), *i.e.* Coulomb interaction, is

$$U_{e-e} = U \sum_{\mathbf{k}, \mathbf{k}', \mathbf{q}} a_{\mathbf{k}+\mathbf{q}}^+ a_{\mathbf{k}'-\mathbf{q}}^+ a_{\mathbf{k}'} a_{\mathbf{k}}. \quad (4.13)$$

The second term of eq. (4.11) is

$$\int \Psi^+(\mathbf{r}) \frac{\omega_0}{K} \sin Kx \frac{1}{i} \frac{\partial}{\partial y} \Psi(\mathbf{r}) d\mathbf{r} \quad (4.14)$$

$$= \sum_k \frac{\omega_0}{K} \frac{k_y}{2i} \{ a_{\mathbf{k}+\mathbf{k}}^+ a_{\mathbf{k}} - a_{\mathbf{k}-\mathbf{k}}^+ a_{\mathbf{k}} \} \quad (4.15)$$

$$\mathbf{K} = \begin{pmatrix} K = \frac{2\pi}{a} \\ 0 \end{pmatrix}. \quad (4.16)$$

Then, eq. (4.11) takes the form

$$H' = \sum_k \frac{\omega_0}{K} \frac{k_y}{2i} \left\{ a_{\mathbf{K}+\mathbf{k}}^+ a_{\mathbf{k}} - a_{\mathbf{k}-\mathbf{K}}^+ a_{\mathbf{k}} \right\} + U \sum_{\mathbf{k}, \mathbf{k}', \mathbf{q}} a_{\mathbf{k}+\mathbf{q}}^+ a_{\mathbf{k}'-\mathbf{q}}^+ a_{\mathbf{k}'} a_{\mathbf{k}}. \quad (4.17)$$

The excess conductivity  $-\Delta\sigma$  calculated for the first term in eq. (4.17), which corresponds to the  $C$ -term ( $\Delta\rho = AT^2 + C$ ), is given as

$$-\Delta\sigma(T=0) = \frac{e^2}{h} (\omega_0\tau)^2 \frac{\sqrt{k_F^2 - (K/2)^2}}{K} \quad K = 2\pi/a \quad (4.18)$$

where  $\Delta\sigma \equiv \sigma_{xx} - \sigma_0 = 1/\rho_{xx} - 1/\rho_0$ . As  $k_F \gg K$  in the present experimental configuration, we can expect that  $-\Delta\sigma$  is proportional to  $B_0^2\tau^2\sqrt{n_e}$  from eq. (4.18).

By illuminating with an LED, we changed the density  $n_e$  of the single sample. Figure 4.6 shows that  $-\Delta\sigma$  at  $T=0$  is plotted against  $B_0^2\tau^2\sqrt{n_e}$ . The data shows quite good agreement with the theoretically calculated result.

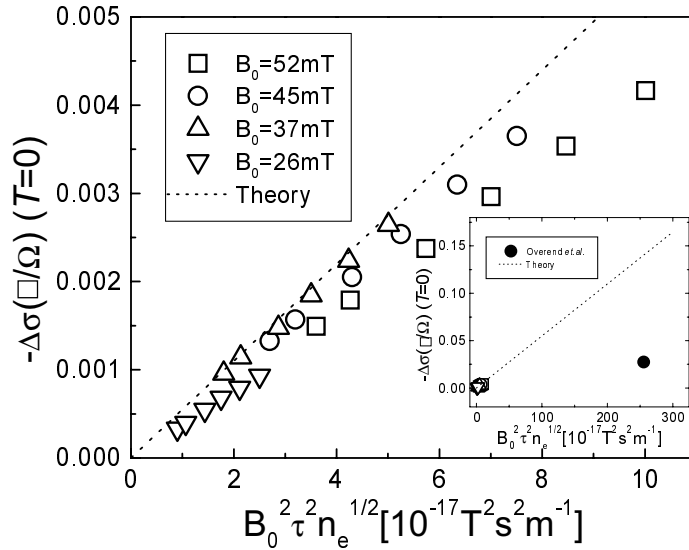


**Figure 4.6:**  $-\Delta\sigma$  at  $T=0$  is plotted against  $B_0^2\tau^2\sqrt{n_e}$ . Dotted line shows theoretically calculated result eq. (4.18). The inset shows the data obtained by Overend *et al.* [6]. Electron density  $n_e = 4.5 \times 10^{15} \text{ m}^{-2}$ , mobility  $\mu = 55 \text{ m}^2 \text{ V}^{-1} \text{ s}^{-1}$ , modulation period  $a = 0.5 \mu\text{m}$ , and modulation amplitude  $B_0 = 300 \text{ mT}$  for the device used in [6]

At finite temperatures, the electron-electron scattering due to the second term in eq. (4.17) also contributes to the conductivity. Although the e-e scattering time  $\tau_{e-e} \propto T^2 \ln(E_F/k_B T)$  in a two-dimensional system from

eq. (4.7), the conductivity itself shows  $T^2$ -dependence. Sasaki *et.al.* shows that

$$\begin{aligned}\Delta\sigma &= -A_{e-e}T^2 \\ A_{e-e} &\equiv \frac{\pi^2 e^2}{6} \frac{e^2}{h} (UD)^2 \left(\frac{e}{m}\right)^2 \frac{(k_B)^2}{\hbar^3 K^2} \times B_0^2 \tau^3.\end{aligned}\quad (4.19)$$

Here,  $D$  is the density of states of the Fermi energy. Figure 4.7 shows the  $B_0^2$ -dependence of  $A_{e-e}$ . The coefficient of the  $T^2$ -term associated with the e-e scattering rate should be proportional to the square of the transition matrix element,  $B_0^2$ . From eq. (4.19),  $A_{e-e}$  is expected to be proportional to

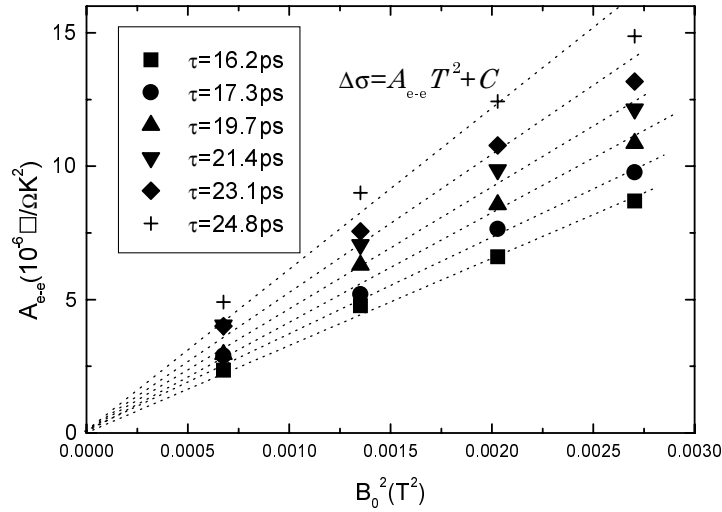


**Figure 4.7:**  $B_0^2$ -dependence of  $A_{e-e}$ .

$B_0^2 \tau^3$ . It is noted that only the value  $U$  can be taken as fitting parameter. Figure 4.8 shows  $B_0^2 \tau^3$ -dependence of  $A_{e-e}$ . The results give us the estimated value  $DU \sim 0.11$ . The plotted data shows some deviation from  $B_0^2 \tau^3$ -dependence. The deviation from the theoretical expectation is presumably originated from the fact we neglect  $q$ -dependence of  $U$  in eq. (4.17), which leads to  $n_e$ -independence of  $U$ . The screening effect qualitatively increases with increasing  $n_e$ , which leads to minimizing the effect of electron-electron interaction. Figure 4.9 shows  $n_e$ -dependence of estimated value  $DU$ . We obtain  $DU \propto 1/n_e$  from the results, however, we hope that the present result may stimulate more efforts on the theoretical side.

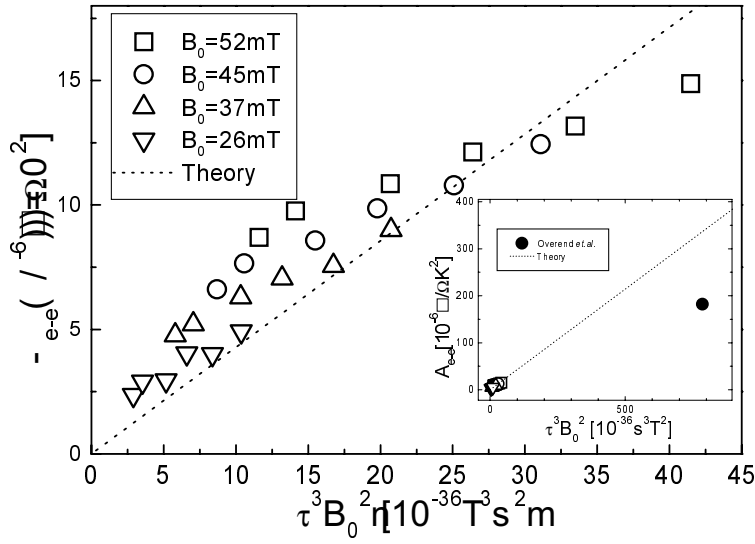


**Figure 4.8:**  $\tau^3 B_0^2$ -dependence of  $A_{e-e}$ . Dotted line shows theoretically calculated result eq. (4.19). The inset shows the data obtained by Overend *et al.* [6]. Electron density  $n_e = 4.5 \times 10^{15} \text{m}^{-2}$ , mobility  $\mu = 55 \text{m}^2 \text{V}^{-1} \text{s}^{-1}$ , modulation period  $a = 0.5 \mu\text{m}$ , and modulation amplitude  $B_0 = 300 \text{mT}$  for the device used in [6]

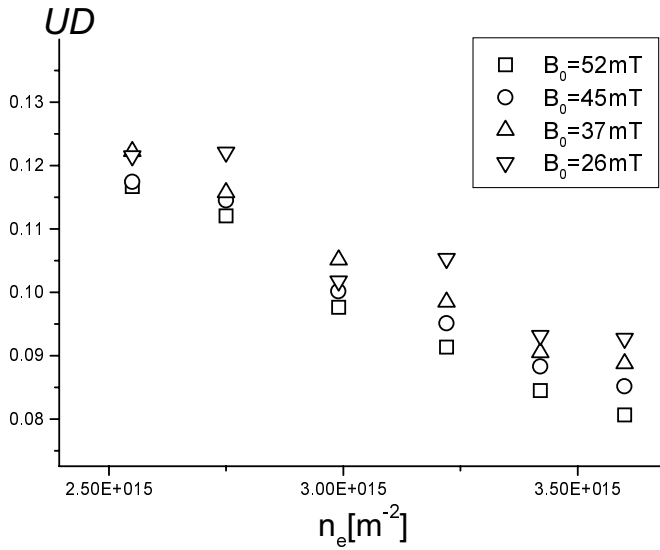


**Figure 4.9:**  $n_e$ -dependence of  $DU$  using eq.(4.19)

It is possible that the amplitude of magnetic field modulation is so large that we are observing the effects of miniband formations. From eq.(4.9), the amplitude of the minigap can be approximately written as  $U_0 = (\omega_0/K)\hbar k_F$  near the Fermi level. The estimated value  $U_0$  is 0.9meV at  $B_0=52\text{mT}$  for the present sample. When the collision broadening  $\hbar/\tau_0$  exceeds  $U_0$ , the collision will wash out the effects. Although the value  $\hbar/\tau_0=0.04\text{meV}$  evaluated from the resistivity is much less than  $U_0$ , our results which show good agreement with the perturbation theory do not exhibit the evidence of miniband formations. It implies that the scattering time relevant to the level broadening is much less than the transport relaxation time  $\tau_0$ . A rough estimate of the relevant scattering time can be made from the threshold magnetic field for the appearance of the SdH oscillation  $\hbar/\tau_0 = 0.5\text{meV}$ .

A similar  $T^2$ -dependent excess resistance is recently reported by Overend *et.al.*[6] for their device with cobalt stripes. The inset of Fig. 4.6 and that of Fig. 4.8 show our data and the results given by Overend *et.al.*[6]. They used the device with electron density  $n_e=4.5\times 10^{15}\text{m}^{-2}$ , mobility  $\mu=55\text{m}^2\text{V}^{-1}\text{s}^{-1}$ , modulation period  $a=0.5\mu\text{m}$ , and modulation amplitude  $B_0=300\text{mT}$ .

## 4.5 Electron temperature dependence of electron-electron scattering

A strong piece of evidence that the excess resistivity is indeed due to electron-electron scattering, is obtained by a study of the hot electron effect. The measurement of excess resistivity similar to that described in Section 4.3 was carried out as a function of bias current density with the sample kept at the lowest temperature (1.25 K). The electron temperature  $T_e$  for low to medium current bias was determined through the standard analysis of the Shubnikov-de Haas (SdH) oscillation amplitude. The comparison between temperature dependence of SdH oscillation with the lowest bias current and the bias current dependence of the oscillation with the lowest temperature gives us the bias current dependence of the electron temperature  $T_e$  at a lower current bias. At a higher current bias, where SdH oscillations are no longer visible, we elected to use the following empirical relationship proposed by Hirakawa and Sakaki [13].

$$P_e = \beta_e(T_e^2 - T_L^2) \quad (4.20)$$

Here,  $T_L$  is the lattice temperature and  $P_e$  is the input power per electron. According to Hirakawa and Sakaki, the coefficient  $\beta_e \approx 2.2 \times 10^{-16} \text{W/K}^2$  is nearly independent of the electron density and mobility. Figure 4.10 shows the results given by Hirakawa et.al. and our results using the present sample. We found that the above relationship holds, with a slightly different value of the coefficient,  $\beta_e \approx 3.5 \times 10^{-16} \text{W/K}^2$ . We used this relationship to estimate  $T_e$  at higher values of bias current.

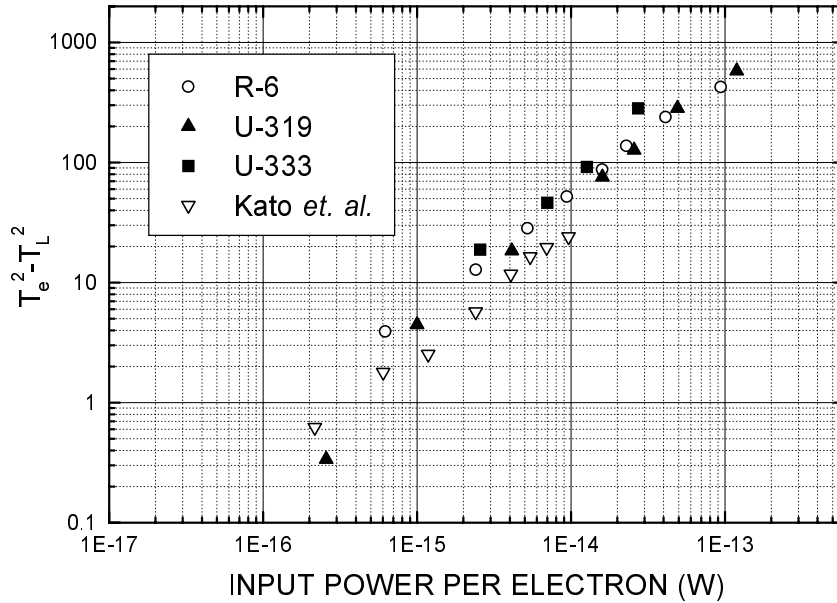


**Figure 4.10:** Input power per electron dependence of  $T_e^2 - T_L^2$  at  $T_L=4.2\text{K}$  given by Hirakawa et.al. [13] and our results at  $T_L=1.5\text{K}$  using the present sample.

The inset of Fig. 4.11 shows the bias current dependence of the resistivity for the  $\varphi = 0^\circ$  ( $B_0=52\text{mT}$ ) and  $\varphi = 90^\circ$  ( $B_0=0$ ) configurations. The current density independence of  $\rho$  for the latter case ensures that the lattice temperature remains unchanged even at the highest bias current. (A change in the lattice temperature would manifest itself as the  $T$ -linear resistivity due to acoustic phonon scattering.) The solid triangles in the main panel of Fig. 4.11 show  $\Delta\rho$  as a function of  $T_e^2$ . It is seen that they are in good agreement with the  $T^2$ -dependence (open squares) taken at low current bias.

This result furnishes an unmistakable piece of evidence that the observed resistivity increase is indeed due to the electron-electron scattering.

We also note that the present result forms a basis for a possible new method of determining the temperature  $T_e$  of hot electrons. An advantage of this method over the more conventional method based on the Shubnikov-de Haas oscillation is that the former can be used at low (or even zero) magnetic fields and can be applied to low-mobility samples.

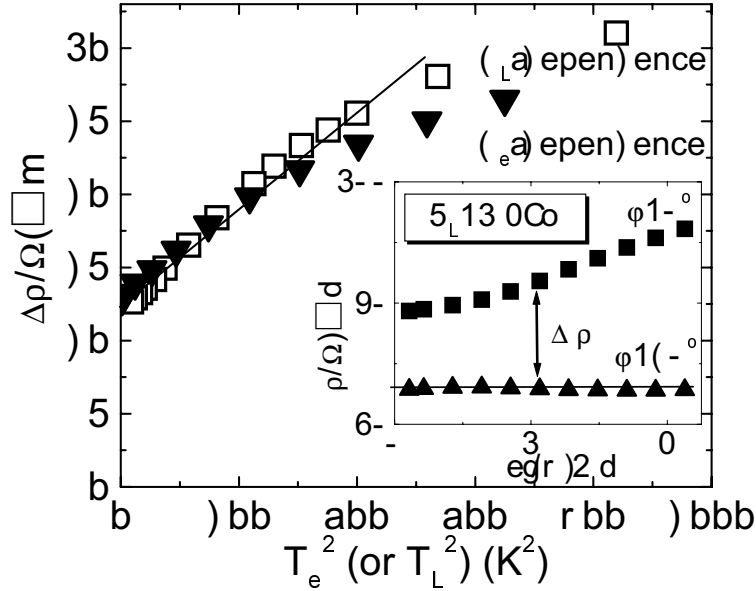


**Figure 4.11:** The inset shows the current density dependence of the resistivity for the  $\varphi = 0^\circ$  ( $B_0=52\text{mT}$ ), and  $\varphi = 90^\circ$  ( $B_0=0$ ) configurations. The main panel shows  $\Delta\rho$  as a function of  $T_e^2$  (solid triangles) to be compared with the  $T^2$ -dependence in the low bias current limit (open squares).

## 4.6 Transverse resistance in oblique lateral superlattice

As shown in the inset of Fig. 4.4 (b), the contribution of e-e scattering to the excess resistivity depends on the angle between modulation wave vector and current direction. The contribution vanishes in the ( $\mathbf{K} \perp \mathbf{J}$ ) sample. When the Umklapp vector was made at an angle  $45^\circ$  with the current vector, the scattering process is expected to contribute equally to the longitudinal and

transverse components of the electric field. We made the Hall bar oriented with the current channel parallel to the  $[110]$  direction, and the grating pattern made of cobalt oriented along the  $[100]$  direction so that the modulation wave vector was at  $45^\circ$  with respect to the current direction as shown in the inset of Fig. 4.12. The reason for setting the grating pattern parallel to the  $[100]$  direction was to minimize the built-in potential modulation due to strain via the piezoelectric coupling as mentioned in Section 2.3 [11, 12]. We measured the longitudinal and transverse resistivity components with an

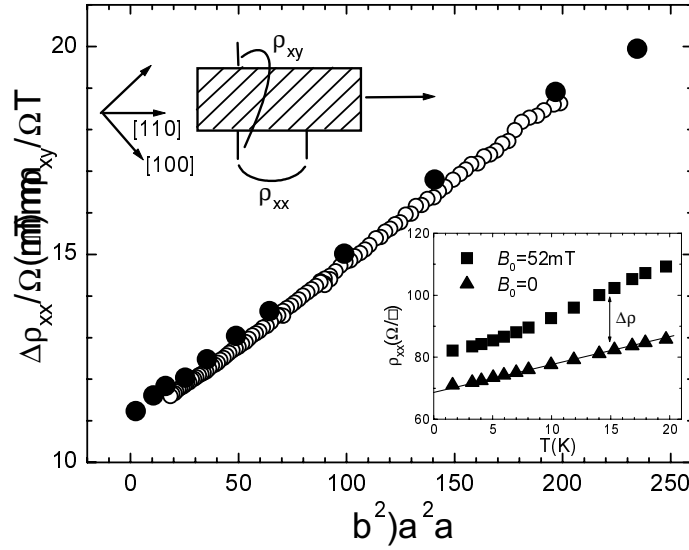


**Figure 4.12:** The upper left inset schematically shows the sample configuration. The lower right inset shows the temperature dependences of the resistivities in the presence and absence of the spatially alternating magnetic field. The difference of the two sets of data gives the excess resistivity  $\Delta\rho_{xx}$  due to the lateral magnetic superlattice. The main panel shows the excess longitudinal resistivity  $\Delta\rho_{xx}$  (solid circles) and the transverse resistivity  $\rho_{xy}$  (open circles) as a function of  $T^2$ .

external field  $B_{\parallel} = 5\text{T}$  applied exactly parallel to the 2DEG plane and parallel to the modulation wave vector (*i.e.* perpendicular to the long side of the strips). The amplitude of the magnetic field modulation for this configuration is  $B_0 \approx 52\text{mT}$ . The effect of the lateral magnetic superlattice in this case manifests itself as an increase in the longitudinal resistivity, and as a non-zero transverse resistivity component even though the uniform component of the magnetic field is zero.

The lower right inset of Fig. 4.12 shows the temperature dependence of the longitudinal resistivity in the presence and absence of the magnetic field modulation. The excess longitudinal resistivity  $\Delta\rho_{xx}$  is defined as the difference between the two data, and is plotted against  $T^2$  in the main panel with solid circles. They obey the relation  $\Delta\rho_{xx}(T) = AT^2 + C$ . Also shown here is the transverse resistivity  $\rho_{xy}$  (open circles), which occurs only in the case of oblique lateral superlattice. It is seen that the relation  $|\rho_{xy}(T)| = \Delta\rho_{xx}(T)$  holds very well in the present case of  $45^\circ$  oblique grating. Numerically,  $|\rho_{xy}(T)| = \Delta\rho_{xx}(T) = 11.0 + 0.040(T[K])^2$  [ $\Omega$ ] for  $B_0 = 52mT$ .

The result,  $|\rho_{xy}(T)| = \Delta\rho_{xx}(T)$ , by itself carries no new information since it can be derived from the anisotropic resistivity tensor with respect to the direction of  $\mathbf{K}$ . However, it is of practical use in the case of electrostatic modulation which we now turn to. For this measurement, we demagnetized the ferromagnetic gate and changed the gate bias at zero magnetic field. The inset of Fig. 4.13 shows the gate bias dependence of  $\rho_{xx}$  and  $\rho_{xy}$  at 1.5 K. With increasing negative gate bias,  $\rho_{xx}$  increases and  $\rho_{xy}$  becomes non-zero, even though no magnetic field is involved at all. The situation here is somewhat more complicated than the case of magnetic modulation, because the gate bias changes not only the electrostatic modulation amplitude but also the electron density, so that the quantity  $\Delta\rho_{xx}$  cannot be extracted so straightforwardly as the case of magnetic modulation. However, in the case of  $45^\circ$  oblique grating, we can estimate the value  $\Delta\rho_{xx}$  using the results of magnetic case  $\Delta\rho_{xx} = |\rho_{xy}|$ .

The main panel of Fig. 4.13 shows  $\rho_{xx}(T)$  and  $\rho_{xy}(T)$  for the gate bias  $V_g = -200mV$ . The electron density at this gate bias determined from the Hall data is  $n_e = 3.2 \times 10^{15}m^{-2}$ , which is a little lower than  $n_e = 3.4 \times 10^{15}m^{-2}$  at  $V_g = 0$ . As seen in the inset, the resistivity change in this range of the gate bias is small, so that the effect of the lateral electric superlattice can be treated as perturbation. It is seen that  $\rho_{xy}(T)$  shows a  $T^2$  dependence, while  $\rho_{xx}(T)$  shows behavior close to  $T$ -linear. Numerically,  $\rho_{xy} = 0.82 + 0.0016 (T[K])^2$  [ $\Omega$ ] for  $V_g = -200mV$ . Based on the result for the lateral magnetic superlattice, we assume that  $|\rho_{xy}(T)| = \Delta\rho_{xx}(T)$ , and evaluate the quantity  $\rho_{xx} - |\rho_{xy}|$ , which corresponds to  $\rho_{xx}^{(0)} = \rho_{xx} - \Delta\rho_{xx}$ , *i.e.* the resistivity excluding the effect of the lateral superlattice, which is shown by small dots in Fig. 4.13. The  $\rho_{xx}^{(0)}$  thus obtained is not so different from  $\rho_{xx}$  for the present case of weak modulation. The temperature dependence of  $\rho_{xx}^{(0)}$

is approximately  $T$ -linear, which attributed to acoustic phonon scattering as mentioned earlier. The coefficient of the  $T$ -linear term of the inverse mobility  $1/\mu$  is calculated as  $\alpha = 3.3 \times 10^{-8} \text{Vs/cm}^2\text{K}$  and is in good agreement with those reported in the literature.[8] We note however that  $\rho_{xx}^{(0)}(T)$  of the 2DEG under electrostatic modulation shows some deviation from the  $T$ -linear behavior of a plain 2DEG.

The deviation from the simple picture becomes more evident, as the gate bias is set more negative. Firstly, the temperature dependence of  $\rho_{xx}^{(0)} = \rho_{xx} - |\rho_{xy}|$  deviates further from the  $T$ -linear behavior and becomes increasingly superlinear. Secondly,  $\rho_{xy}$  at low temperature deviates from the  $T^2$ -dependence. Under a large negative bias,  $\rho_{xy}$  even shows an upturn at the lowest temperatures. These anomalous features are presumably associated with the following. A large negative bias both decreases the Fermi energy and increases the electrostatic modulation amplitude. When the latter is not so small compared to the former, the perturbative treatment breaks down. It is necessary to take account of the spatial inhomogeneity of the electron density. Another factor is that the effect of disorder gains importance with decreasing electron density, In order to interpret the experimental data in the large negative bias region, these factors have to be properly taken into account.

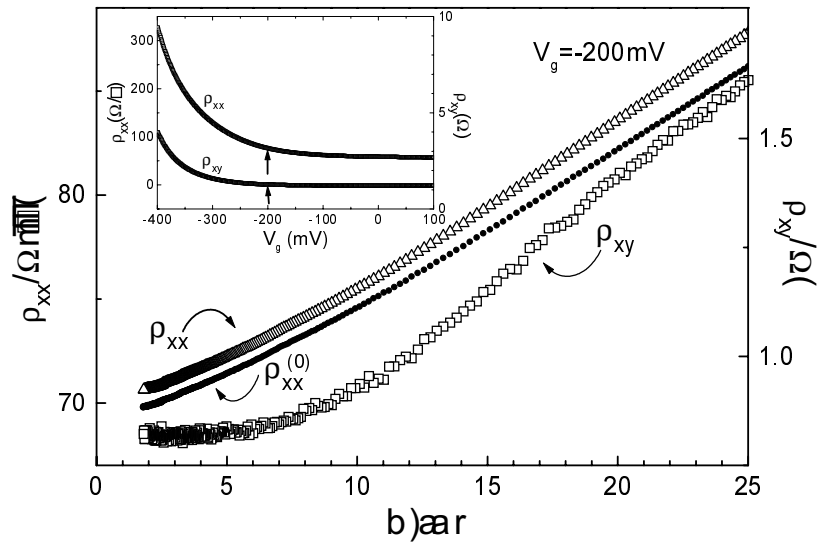


**Figure 4.13:** The inset shows the longitudinal resistivity  $\rho_{xx}$  and the transverse resistivity  $\rho_{xy}$  as a function of the gate bias  $V_g$ . The main panel shows the temperature dependences of  $\rho_{xx}$  (triangles, left scale) and  $\rho_{xy}$  (squares, right scale) with the gate bias fixed at  $V_g = -200 \text{ mV}$  (marked by arrows in the inset). The small dots represent  $\rho_{xx}^{(0)} = \rho_{xx} - |\rho_{xy}|$  which corresponds to the resistivity after subtracting the effect of the lateral superlattice.



# References

- [1] J.M. Ziman: *Electrons and Phonons* (Clarendon Press, Oxford, 1960).
- [2] K. Yamada and K. Yosida: Prog. Theor. Phys. **76** 621 (1986).
- [3] H. Maebashi and H. Fukuyama: J. Phys. Soc. Jpn. **66** 3577 (1997).
- [4] T. Okabe: J. Phys. Soc. Jpn. **67** 2792 (1998).
- [5] A. Messica, A. Soibel, U. Meirav, A. Stern, H. Shtrikman, V. Umansky and D. Mahalu: Phys. Rev. Lett. **78** 705 (1997).
- [6] N. Overend, A. Nogaret, B. L. Gallagher, P. C. Main, R. Wirtz, R. Newbury, M. A. Howson, S. P. Beaumont: Physica B **249-251** 326 (1998)
- [7] G.F. Giuliani and J.J. Quinn: Phys. Rev. **B26** 4421 (1982).
- [8] E. E. Mendez, P. J. Price and M. Heiblum: Appl. Phys. Lett. **45** 294 (1984).
- [9] B. J. F. Lin, D. C. Tsui and G. Weimann: Solid State Commun. **56** 287 (1985).
- [10] T. Sasaki and H. Fukuyama, in preparation.
- [11] E. Skuras, A.R. Long, I.A. Larkin, J.H. Davies, and M.C. Holland, Appl. Phys. Lett. **70** 871 (1997).
- [12] A. Nogaret, S. Carlton, B.L. Gallagher, P.C. Main, M. Henini, R. Wirtz, R. Newbury, M.A. Howson, and S.P. Beaumont, Phys. Rev. **B55** 16037 (1997).
- [13] H. Hirakawa and H. Sakaki, Appl. Phys. Lett., **49** 889 (1986).



# Chapter 5

## Conclusion

We have demonstrated that spatially modulated magnetic field can be imposed on 2DEG at the GaAs/AlGaAs heterointerface in a controlled fashion. Independent control of the field components parallel and perpendicular to the 2DEG plane allowed us to fix the magnetization of the striped ferromagnetic gate, while we measure the low (or zero) magnetic field transport in the 2DEG. The amplitudes of the magnetic and electrostatic modulations can be determined from the analysis of the Weiss oscillation.

The 2DEG under a modulated magnetic field with zero uniform component is of particular interest in the context of combined effect of electron-electron interaction and artificial periodicity. Here, the use of magnetic field modulation in place of ordinary electrostatic modulation has a distinct advantage that the modulation amplitude can be varied without affecting the 2DEG density. The excess resistivity at finite temperatures shows a  $T^2$ -dependence characteristic of the electron-electron interaction. These are manifestation of electron-electron umklapp process, which are brought into play by lifting of Galilean invariance by the artificial lateral superlattice. The results given by the study of hot electron and oblique lateral superlattice also support this picture. The present system offers an ideal ground for quantitative comparison between theory and experiment for this fundamental issue of solid state physics.

## Acknowledgement

I would like to express my sincere thanks to Prof. Y. Iye for his continual guidance and encouragement, for providing nice working conditions and for his helpful comments throughout the course of present work.

I am also grateful to Prof. S. Katsumoto who gave me useful advice and valuable discussions.

I thank Mr. T. Sasaki and Prof. H. Fukuyama for helpful conversations.

The present work owes much to their advice and useful discussions of Dr. A. Endo, Dr. K. Kobayashi and Dr. M. Hirasawa.

To everybody who's a part of ISSP, especially Iye and Katsumoto laboratory; staffs and my colleagues who cheered me up and helped my work even late nights and mornings, I know I don't get to say this often, so...."Thank you very much !"

To my friends (you should know who you are !), thanks for your love and support.

And to my family, I want you to know *how much I thank you*.

I wish to thank the support by the Research Fellowship of the Japan Society for the Promotion of Science. This work was supported by the Grant-in Aid for Scientific Research from the Ministry of Education, Science, Sports and Culture, and the Core Research for Evolutionary Science and Technology (CREST) Program of the Japan Science and Technology Corporation.

To everyone who's reading this, I dedicate this thesis to all of you!

*Mayumi Kato*